isvr Institute of Sound and Vibration Research

Active Vibration Isolation of a Flexible Equipment Structure on a Flexible Base

X. Huang, S.J. Elliott and M.J. Brennan

ISVR Technical Memorandum 879

October 2001

University of Southampton

SCIENTIFIC PUBLICATIONS BY THE ISVR

Technical Reports are published to promote timely dissemination of research results by ISVR personnel. This medium permits more detailed presentation than is usually acceptable for scientific journals. Responsibility for both the content and any opinions expressed rests entirely with the author(s).

Technical Memoranda are produced to enable the early or preliminary release of information by ISVR personnel where such release is deemed to the appropriate. Information contained in these memoranda may be incomplete, or form part of a continuing programme; this should be borne in mind when using or quoting from these documents.

Contract Reports are produced to record the results of scientific work carried out for sponsors, under contract. The ISVR treats these reports as confidential to sponsors and does not make them available for general circulation. Individual sponsors may, however, authorize subsequent release of the material.

UNIVERSITY OF SOUTHAMPTON

INSTITUTE OF SOUND AND VIBRATION RESEARCH

SIGNAL PROCESSING & CONTROL GROUP

Active Vibration Isolation of a Flexible Equipment Structure on a Flexible Base

by

X Huang, S J Elliott and M J Brennan

ISVR Technical Memorandum N° 879

October 2001

Authorised for issue by
Prof S J Elliott
Group Chairman

Table of Contents

Abstract

This report investigates the dynamic characteristics and control mechanisms of an active vibration isolation system for a flexible equipment structure attached by four mounts to a flexible base structure. Decentralised velocity feedback control is applied, in which each of the four actuators is operated independently by feeding back the absolute equipment velocity signal at the corresponding mount location. Passive mounts are modelled as lumped parameter springs and dampers as far as the isolation of low frequency vibration is investigated, but the flexible modes of the equipment structure must also be considered. The dynamic characteristic behaviour of the coupled system is analyzed theoretically using the impedance method. A multichannel control system for the active isolation of a flexible equipment structure from a vibrating base, as well as various single channel control systems, has been implemented experimentally. The measured equipment velocity responses and closed loop attenuations from the experiments are in good agreement with the predicted results. Good stability properties are predicted from the simulations and verified in the experiments. Control performances of the single channel and multichannel control implementations are assessed both theoretically and experimentally in terms of absolute equipment velocity response as well as the kinetic energy represented by the sum of the squared values of the equipment velocities at the mount positions. A single channel controller is effective in attenuating vibrations at all the resonance frequencies of the mounted equipment structure, while a global reduction in vibration level is achieved at all resonance frequencies of the coupled system if a four-channel controller is implemented in practice. In particular, up to 25 dB reduction in the kinetic energy at the rigid body modes of the mounted equipment structure, as well as up to 20 dB reduction at the resonances caused by the low order flexible modes of the coupled base and equipment structure, was achieved in the experiment.

1 Introduction

Isolating a piece of delicate equipment from the vibration of a base structure is of practical importance in various engineering fields. Examples are the vibration isolation of the instrument boxes in an aeroplane and the isolation of telescopes in satellites. In the majority of cases, the base is flexible and vibrates with an unpredictable waveform which has a broadband spectrum. Passive anti-vibration mounts are widely used to support the sensitive equipment structure and protect it from severe base vibration. However, conventional passive mounts suffer from an inherent trade-off between high frequency isolation and amplification of vibration at the basic mounted resonance frequency [1]. Generally the best isolation performance is achieved by coupling an active system in combination with a passive mount, where the basic resonance can be actively controlled without reducing the high frequency performance at all frequencies of interest.

An active isolation system can be implemented over a broad frequency band using feedback control strategies, among which velocity feedback control is one of the most popular. The absolute velocities of the equipment structure is measured at each mounting point and directly fed back to the actuators driving that point. If the secondary force generated by the active system acts in proportion to the absolute velocity of the equipment, the feedback control is equivalent to adding damping in the passive isolator without compromising the high frequency isolation performance. Such a control strategy is well-established and termed as skyhook damper in the literature [1]. An experimental study was conducted by Serrand and Elliott [2] on the active vibration isolation of a rigid equipment structure using two electromagnetic shakers, which were installed in parallel with two passive mounts. Using independent velocity feedback control, Kim et al [3] investigated a four-mount active vibration isolation system with a rigid equipment structure.

This report investigates the active isolation of a flexible equipment structure from the vibration of a flexible base structure. The objective is to study the performance and control stability issues associated with the active vibration isolation system when additional flexibility of the equipment structure is introduced. Particular emphasis is placed on the isolation of low frequency vibration (0~200Hz), for which the mounts can be assumed to behave as lumped springs and dampers. A general theoretical model is derived using the impedance method to investigate the dynamic behaviour of the coupled system in section 2. Section 3 presents simulations for the dynamic behaviour of the coupled flexible equipment and base structures. A description on the experimental apparatus and implementation of the active vibration isolation system is given in section 4, and the theoretical model is validated experimentally in section 5. Control stability of the active isolator is evaluated theoretically and experimentally in section 6 before the decentralised feedback control strategy is implemented experimentally in the active vibration isolation system. The performances of a single channel and multichannel active vibration control systems with a flexible equipment structure on a flexible base structure are then discussed in section 7 and section 8 summarizes the conclusions.

2 Theoretical analysis of the mounted equipment structure

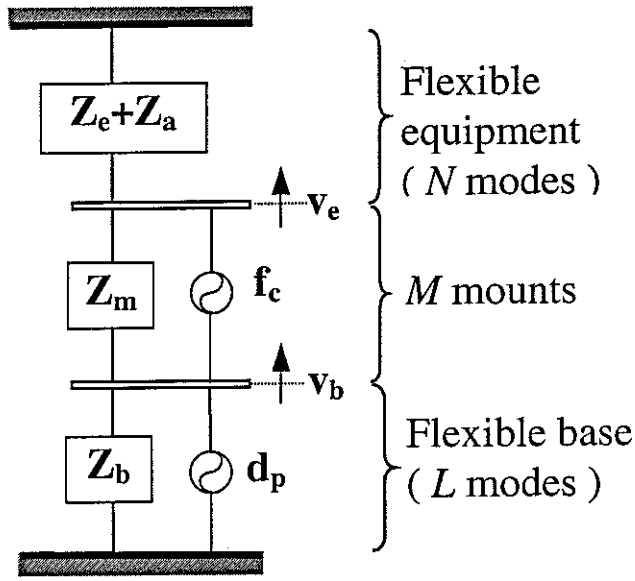

Figure1. Impedance representation of a multi-mount active vibration isolation system

A detailed theoretical analysis of the active vibration isolation system, where a piece of flexible equipment is supported by a set of mounts on a flexible base, has been given in a previous report [4] using the impedance method. As a result, only a brief description is given here. The mounted flexible equipment structure can be represented in terms of impedances as shown in Figure 1. The number of mounts under consideration is set to be M, and the total number of modes in the flexible equipment is N. Compared to the mass of the equipment and the actuators, the mounts are assumed as massless. The end velocities at the mount positions are denoted as an M length vector $\mathbf{v}_e$ for the flexible equipment structure, while an M length secondary force vector $\mathbf{f}_c$ denotes the control forces generated by the actuators. Assuming that the flexible base structure is excited by a primary force vector $\mathbf{f}_p$, the dynamic behaviour of the multi-mount active vibration isolation system of a flexible equipment structure on a flexible base can be described in matrix form as follows,

$$\begin{bmatrix} \mathbf{Z}_e + \mathbf{Z}_a + \mathbf{Z}_m & -\mathbf{Z}_m \\ -\mathbf{Z}_m & \mathbf{Z}_b + \mathbf{Z}_m \end{bmatrix} \begin{Bmatrix} \mathbf{v}_e \\ \mathbf{v}_b \end{Bmatrix} = \begin{Bmatrix} \mathbf{f}_c \\ \mathbf{d}_p - \mathbf{f}_c \end{Bmatrix} \tag{1}$$

where, $\mathbf{Z}_a$, $\mathbf{Z}_e$ and $\mathbf{Z}_m$ denote the impedance matrixes of the actuators, the flexible equipment and the mounts, respectively. In particular, $\mathbf{Z}_a$ and $\mathbf{Z}_m$ are (M×M) diagonal matrixes, whose elements are the impedances due to the mass of each actuator, and the stiffness and damping of the corresponding mount respectively. $\mathbf{d}_p = \mathbf{Z}_b \mathbf{Y}_{bp} \mathbf{f}_p$, in which $\mathbf{Y}_{bp}$ is the mobility matrix of the uncoupled flexible base due to the primary force vector $\mathbf{f}_p$.

At low frequencies, the control force generated from the electromagnetic actuator is approximately proportional to the input velocity signal. If direct velocity feedback control is employed which uses the absolute velocity signal $\mathbf{v}_e$ of the flexible

equipment structure to activate the actuators with constant gain matrix of $-\mathbf{H}$, the control force vector $\mathbf{f}_c$ generated by the actuators is,

$$\mathbf{f}_c = -\mathbf{H}\mathbf{v}_e \tag{2}$$

When decentralised feedback control is employed, each of the actuators is operated independently by feeding back the absolute equipment velocity with the same gain at each mount location. The feedback gain matrix is then diagonal. Therefore, the dynamic response of the couple active isolation system is obtained by substituting equation (2) into (1) to give,

$$\begin{bmatrix} \mathbf{Z}_e + \mathbf{Z}_a + \mathbf{Z}_m + \mathbf{H} & -\mathbf{Z}_m \\ -(\mathbf{H} + \mathbf{Z}_m) & \mathbf{Z}_b + \mathbf{Z}_m \end{bmatrix} \begin{Bmatrix} \mathbf{v}_e \\ \mathbf{v}_b \end{Bmatrix} = \begin{Bmatrix} \mathbf{0} \\ \mathbf{d}_p \end{Bmatrix} \tag{3}$$

Conventionally, control performance is discussed in terms of transmissibility, which is defined by v_e/v_b for a single mount active isolation system. However, the dynamic behaviour of the mounted flexible equipment structure is strongly coupled with the dynamics of the flexible base structure as indicated from equation (3). The control force changes the base velocity, which in turn affects the velocity of the flexible equipment structure. Therefore, the transmissibility does not represent the absolute vibration response of the flexible equipment structure. As a result, the absolute velocity of the mounted flexible equipment structure is more preferable as a control performance measure for the mounted active isolation system as discussed in a previous report [4]. The kinetic energy of a rigid equipment structure was suggested as a good measure of control performance [3]. Considering the flexibility of the equipment structure in this research, an approximate estimate of the kinetic energy represented by the sum of squared velocities at all mount locations on the flexible equipment structure will be calculated, and a comparison between the experiment and simulation can be performed to assess the control performance of the active vibration isolation system.

3 Simulation of a four-mount active isolation system on a flexible base structure

Without losing generality, simulations are performed for an active vibration isolation of a flexible equipment structure attached by four mounts to a flexible base structure, in which four electromagnetic actuators are installed in parallel with four passive mounts as shown in Figure 2. The flexible equipment structure in the simulation is a uniform aluminium plate of 3.54 mm thickness. A thin rectangular steel plate of 2 mm thickness, which is clamped along the two long opposite edges and free at the other two, is modelled as the supporting flexible base structure. In the simulation, both the equipment and base plates are modelled using a modal approach, assuming an isotropic thin flat plate with beam shapes of equivalent boundary conditions as defined by Warburton [5]. Four identical passive mounts are assumed to be massless, and are modelled as parallel connections of springs and dampers in the simulation as far as isolation of low frequency vibration (0~200 Hz) is concerned. Relevant physical and geometry properties of the whole system used in the simulation are tabulated in

Table 1. The stiffness and damping properties of the passive mounts are chosen to best fit the measured natural frequency and bandwidth from the experiments. For the convenience of description, locations of the four mounts are denoted as nodes 1, 2, 3, 4 as shown in Figure 2.

When the flexible equipment structure on a flexible base is excited by one of the control actuators via a white noise signal, the velocity responses of the coupled system can be obtained by setting $\mathbf{d}_p = \mathbf{0}$ in equation (1),

$$\begin{Bmatrix} \mathbf{v}_e \\ \mathbf{v}_b \end{Bmatrix} = \begin{bmatrix} \mathbf{Z}_e + \mathbf{Z}_a + \mathbf{Z}_m & -\mathbf{Z}_m \\ -\mathbf{Z}_m & \mathbf{Z}_b + \mathbf{Z}_m \end{bmatrix}^{-1} \begin{Bmatrix} \mathbf{f}_c \\ -\mathbf{f}_c \end{Bmatrix} \tag{4}$$

where, $[\ ]^{-1}$ is the inverse of the impedance matrix of the coupled system. The plant velocity response matrix of the active vibration isolation system on a flexible base structure can be calculated if vector $\mathbf{f}_c$ takes each column vector from the following matrix consecutively,

$$\begin{bmatrix} 1 & 0 & 0 & 0 \\ 0 & 1 & 0 & 0 \\ 0 & 0 & 1 & 0 \\ 0 & 0 & 0 & 1 \end{bmatrix} \tag{5}$$

Let G_{ij} denote the velocity response at the ith mount location due to a unit force excited at the jth mount location. The magnitudes of predicted plant velocity responses as well as the phase angles are shown in dashed lines in Figure 4 to Figure 19 (dB ref.=10^{-5} m/s). Each peak in the plant velocity responses corresponds to a resonance frequency of either a rigid or a flexible mode of the whole system. Each motion can be clearly distinguished by comparing the other plant frequency responses and checking the corresponding phases at that particular frequency. The first three peaks noticeable in the driving point frequency responses are related to the rigid body modes of the mounted equipment structure according to an initial study of the active vibration isolation system on a rigid base structure [4]. Different from the case of a rigid base structure, three rigid body modes can be distinguished since the flexible base structure provides different values of structural damping to each rigid body mode. In particular, the heave mode is shifted down to 14.3 Hz from 17.40 Hz, pinch mode to 16.0 Hz from 17.78 Hz and roll mode to 17.2 Hz from 17.42 Hz respectively, since the active isolator system is strongly coupled to the flexible base structure which lowers the effective stiffness of the mounted equipment structure. The fourth peak noticeable in Figure 4, which occurs at 43.2 Hz, is related to one of the resonance frequencies of the uncoupled base structure. The frequencies of the flexible modes of the mounted flexible equipment structure are almost the same as the predictions for a rigid base case with the first at around 50.5 Hz and the second at around 131.7 Hz. The overall response drops with increasing frequency as the passive mounts become more efficient. The theoretical analysis can be validated through a detailed comparison with the measured velocity responses of the mounted flexible equipment structure on a flexible base from the experiment, which is described in the following section.

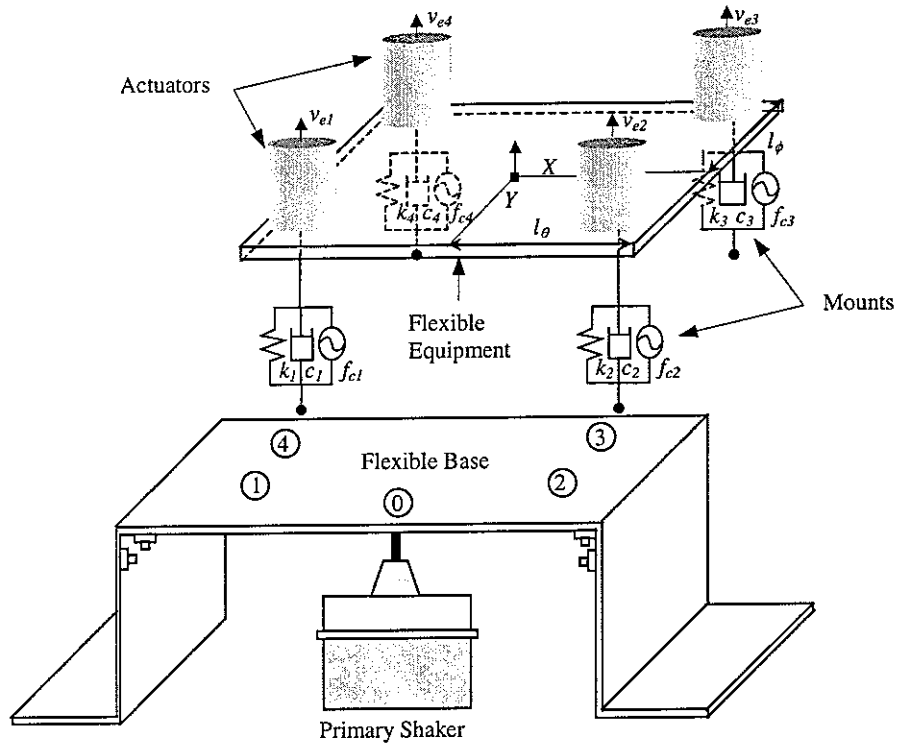

Figure 2. A four-mount active isolator with a flexible equipment structure on a flexible base

Table 1. Physical properties and geometric data of the active isolation system

Equipment Structure	Material of the flexible equipment plate	Aluminium
	Density of the flexible equipment plate	2700 kgm^{-3}
	M_e, Mass of the flexible equipment plate	0.3564 kg
	Young's Modulus	7.1×10^{10} Nm^{-2}
	Poisson's Ratio	0.33
	Damping ratio	$\zeta_e = 0.01$
	Dimensions of the flexible equipment plate (mm) ($L_{ex}\times L_{ey}\times t_e$)	$(300 \times 160 \times 3.54)$
Mount	k_m, spring stiffness of each mount	1.2×10^4 N/m
	c_m, Damping of each mount	11.5 Ns/m
	Mount locations on the flexible equipment (mm)	$l_\theta = 117$, $l_\phi = 47$
Base Plate	Material	Steel
	Dimensions of the flexible base plate (mm) ($L_{bx}\times L_{by}\times t_b$)	$(700 \times 500 \times 2)$
	Damping ratio	$\zeta_b = 0.01$
Actuator	M_a, Mass of each actuator	0.91 kg
Location of Node 1 on the base plate (mm)		$(L_{bx}/2, L_{by}/2)$
Location of the primary force on the base plate (mm)		(320, 270)

4 Experimental implementation of the four-mount active isolator on a flexible base structure

The four-mount active vibration isolation system was built in the laboratory and is illustrated in Figure 2. It consists of a flexible equipment structure mounted on a flexible base plate though four anti-vibration mounts. For the convenience of description, the flexible equipment to be isolated together with the passive and active isolators is referred as the mounted equipment structure. The passive mounts are made of natural rubber with a hollow cylindrical shape. In the experimental setup, the four passive mounts are bonded symmetrically underneath the equipment plate via steel washers, while four electromagnetic shakers are installed rigidly on the top of the equipment plate at the corresponding mount positions by a set of bolts. A thin steel stinger inside each ring mount transmits the axial force generated by the control shakers to the supporting flexible base via an aluminium disc, so that the control force can act in parallel with the passive isolator as in the simulation. The assembly of the experimental set-up is illustrated schematically in Figure 3. It is noted that the control shakers are of Ling type V101 electro-dynamic vibration generators, which can generate a maximum force of 8.9 N. The force generated is proportional to the product of the instantaneous current in the coil and the magnetic flux density. In the low frequency range within 200 Hz, the input voltage to the shaker is proportional to the current in the moving coil as the inductance effect is negligible compared to the shaker electrical resistance. In the frequency range of interest, the motional impedance of each shaker is negligible compared to the blocked impedance. Therefore, the control force generated from the shaker is proportional to the input current and thus to the input voltage. In particular, the control force is proportional to the input velocity signal as velocity feedback control is employed. A steel rectangular plate is designed to have sufficient rigidity to support the mounted equipment structure, whose two long opposite edges are bolted on stiff frames and the others remain free to realise the

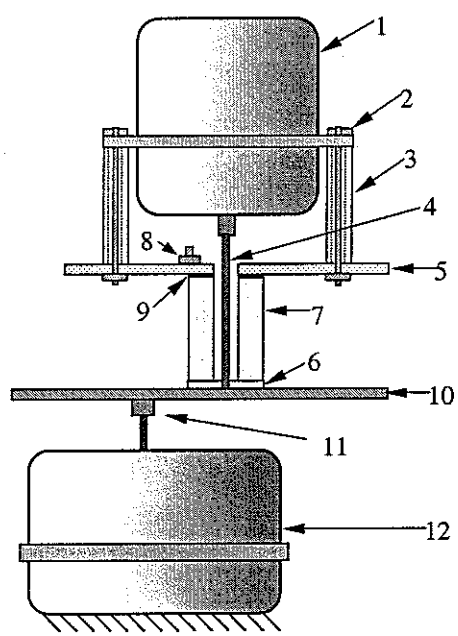

1 Electromagnetic Actuator
2 Bolt
3 Support (height = 40 mm)
4 Stinger
5 Flexible Equipment Structure (Al)
6 Adapter (Al)
7 Rubber Mount (height = 30 mm,
(outer dia. = 30mm, inner dia. = 10 mm)
8 Accelerometer
9 Steel Washer
10 Flexible Base (Steel)
11 Force Gauge
12 Primary Shaker

Figure 3 Assembly of the active isolation system in the experiment

clamped- free - clamped -free boundary conditions as used in the simulation. A primary shaker driven underneath the base plate provides a sufficient velocity signal to avoid any possible signal to noise problems in the experiment. The physical and geometrical properties of the experimental set-up, as well as the locations of the mounts, are the same as those in the simulation as shown in Table 1.

In the experiment, an FFT analyzer (Advantest R9211C) was used to measure the velocity response of the equipment as well as generate the white noise signal. The white noise signal drove the primary shaker to excite the base plate, and the excitation force signal was measured by a force transducer (B&K type 8200) connected to channel A of the analyzer. When the mounted flexible equipment structure was excited, the acceleration signal at each mount location was measured via an accelerometer (B&K type 4375). The acceleration signal was then passed to a general signal conditioner (B&K type 2635) and converted to a velocity signal by an integrated module inside the signal conditioner. The integrator was operated in conjunction with a highpass filter, whose cutoff frequency was preset to be 1 Hz. Finally the velocity signal was inputted into channel B of the analyzer to measure the frequency response function of the absolute equipment velocity per unit excitation force. A built-in filter in the analyzer was employed to reduce aliasing.

The velocity responses of the mounted flexible equipment structure on a flexible base were measured in the experiment and are shown as solid lines in Figures 4 to 19. In order to match the first flexible resonance of the equipment velocity response measured from experiment, the thickness of the flexible equipment plate in the theoretical model was modelled as 2.9 mm rather than 3.54 mm. This lowers the frequency of the first flexible mode of the active isolator and is thought to compensate for the frequency lowering effect of the rotational moments of inertia of the shakers in the experimental arrangement, which were not accounted for in the theoretical model. The first three peaks noticeable in the driving point experimental velocity responses are the rigid body modes of the mounted equipment structure. In particular, the heave mode occurs at about 14.0 Hz, pitch mode at about 16.3 Hz and roll mode at about 18.0 Hz respectively. The fourth peak noticeable in Figure 4 is related to a resonance frequency of the base plate, which occurs at 37.8 Hz. The frequencies of the flexible modes of the mounted flexible equipment structure are almost the same as the predictions for a rigid base case with the first at round 50.5 Hz, the second at around 142.1 Hz and the third at around 190.7 Hz. Stability analysis of the active vibration control of the mounted equipment structure on a flexible base could be assessed when the velocity response matrix of the active isolation system was obtained both theoretically and experimentally.

5 Model validation

Matching the results of a theoretical model to measurements from experiment is a good way of evaluating the degree of confidence in using the theoretical model to predict the dynamics of the mounted flexible equipment structure, assuming all the parameters affecting the system are properly considered. In addition, it is a powerful tool for interpreting and understanding experimental results as it superposes a theoretical background to the phenomena observed from the experiment. Therefore, the plant frequency responses from the simulations (dashed line) were compared with the experimental results (solid line) and shown in Figures 4 to 19 in order to validate the theoretical model developed in section 2.

The measured resonance frequencies of the mounted equipment structure on a flexible base structure were compared both theoretically and experimentally as shown in Table 2. In particular, the measured natural frequencies of the rigid body modes (14.0, 16.3 and 18.0 Hz) are reasonably close to the predicted results from the simulations (14.3 Hz, 16.0 Hz and 17.2 Hz). The first flexible resonance frequency of the mounted equipment structure predicted from the simulation is almost the same to the corresponding experimental result, as the thickness of the equipment is adjusted to best fit the experimental result in the simulations. The resonance of the second flexible mode of the mounted equipment structure occurred at 142.1 Hz in the experiment, which was predicted to be around 131.7 Hz from the simulations. In the experiment, a third flexible mode of the mounted equipment structure was observed at about 190 Hz, which was not predicted by the simulations in the frequency range. The experimental measurements of velocity responses have some discrepancies at frequencies below 10 Hz compared with the simulations, which suffer from the poor coherence due to the low sensitivity of the actuators and the sensor used in the experiment. The dynamics of the flexible base structure is strongly coupled with the mounted equipment structure, and the other peaks over 30 Hz appeared in the velocity responses are related to the resonance frequencies of the flexible base structure. For example, these occur at about 40 Hz and 62 Hz. For the base resonance frequencies, the experiments have some discrepancies in comparison with the theory. In particular, the measured resonance frequencies of the base structure are somewhat lower than the predicted results from the simulation, which is thought because of the imperfect realisation of the clamped-clamped boundary condition in the experiment. The arrangement to fix the base plate does not completely clamp the two longest edges at low frequencies, which acts to reduce the system stiffness and therefore shifting down the natural frequencies of the flexible base structure. The simulation results are otherwise in good agreement with the experimental measurements. The dynamics of the four-mount flexible equipment structure can be thus investigated to within a satisfactory accuracy using the theoretical model outlined in the previous section.

Table 2. Natural frequencies of the mounted flexible equipment structure

Simulation								Experiment					
Frequency (Hz)	Motion	Mode shape				Frequency (Hz)	Motion	Mode shape			
		1	2	3	4			1	2	3	4
14.3	Heave	+	+	+	+	14.0	Heave	+	+	+	+
16.0	Pitch	+	-	-	+	16.3	Pitch	+	-	-	+
17.2	Roll	+	+	-	-	18.0	Roll	+	+	-	-
50.5	Flexible (Torsion)	+	-	+	-	50.5	Flexible (Torsion)	+	-	+	-
131.7	Flexible (Heave)	+	+	+	+	142.1	Flexible (Pitch)	+	-	-	+
						190.7	Flexible (Torsion)	+	-	+	-

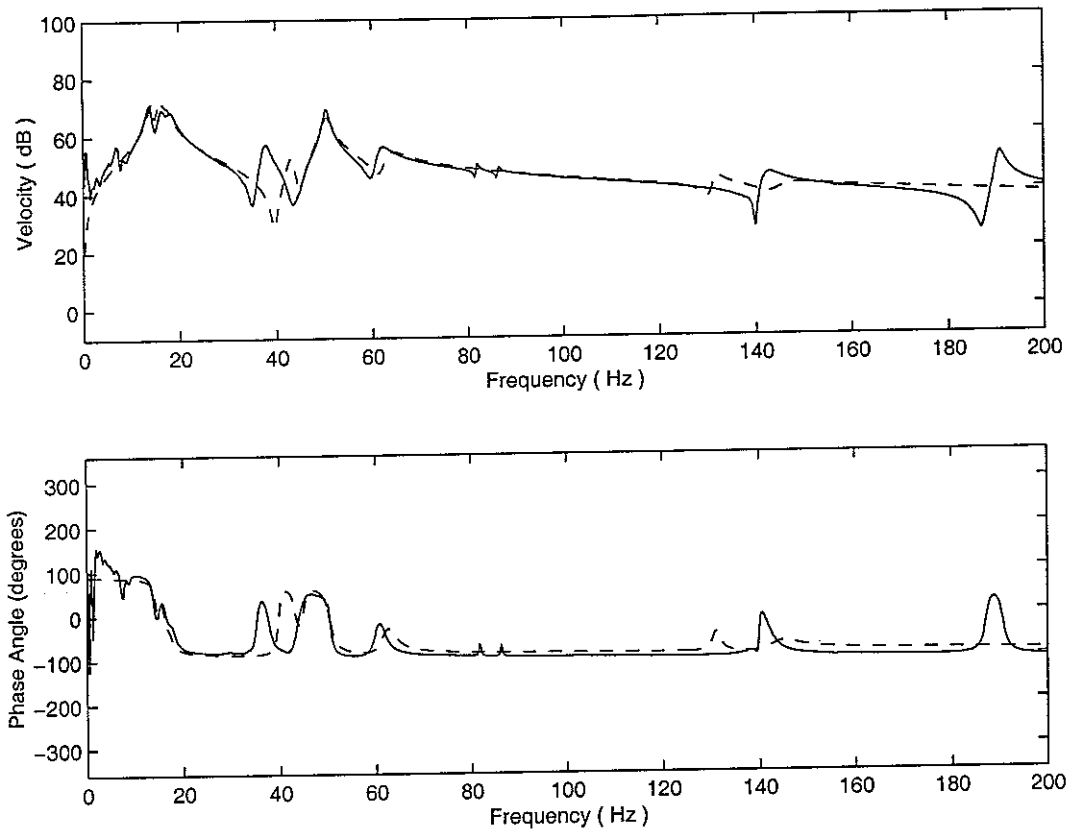

Figure 4 Comparison of plant response G_{11} from simulation (—) and experiment (—)

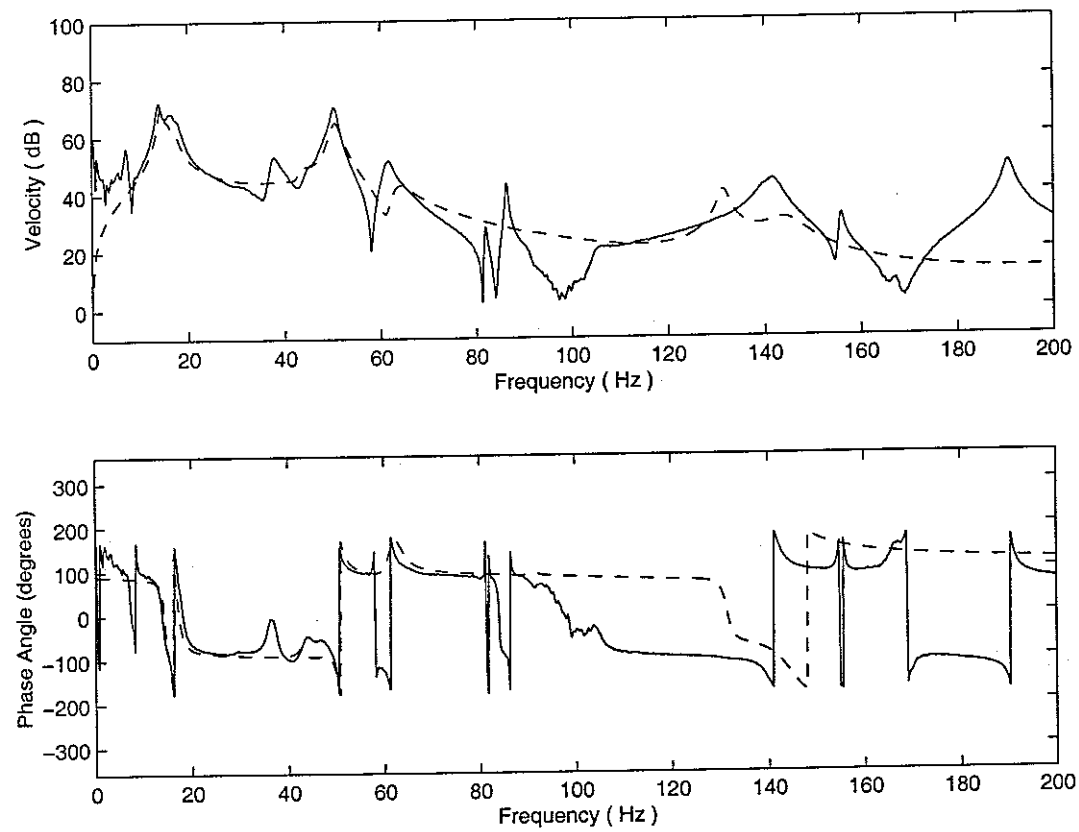

Figure 5 Comparison of plant response G_{12} from simulation (—) and experiment (—)

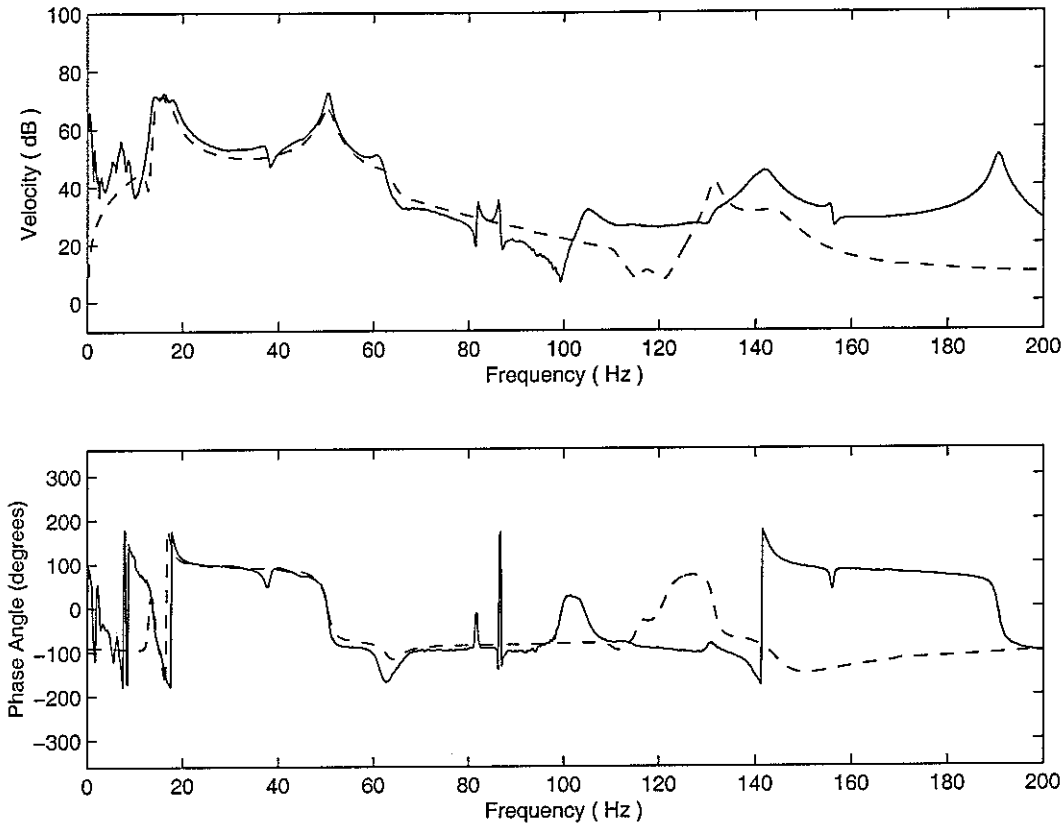

Figure 6 Comparison of plant response G_{13} from simulation (—) and experiment (—)

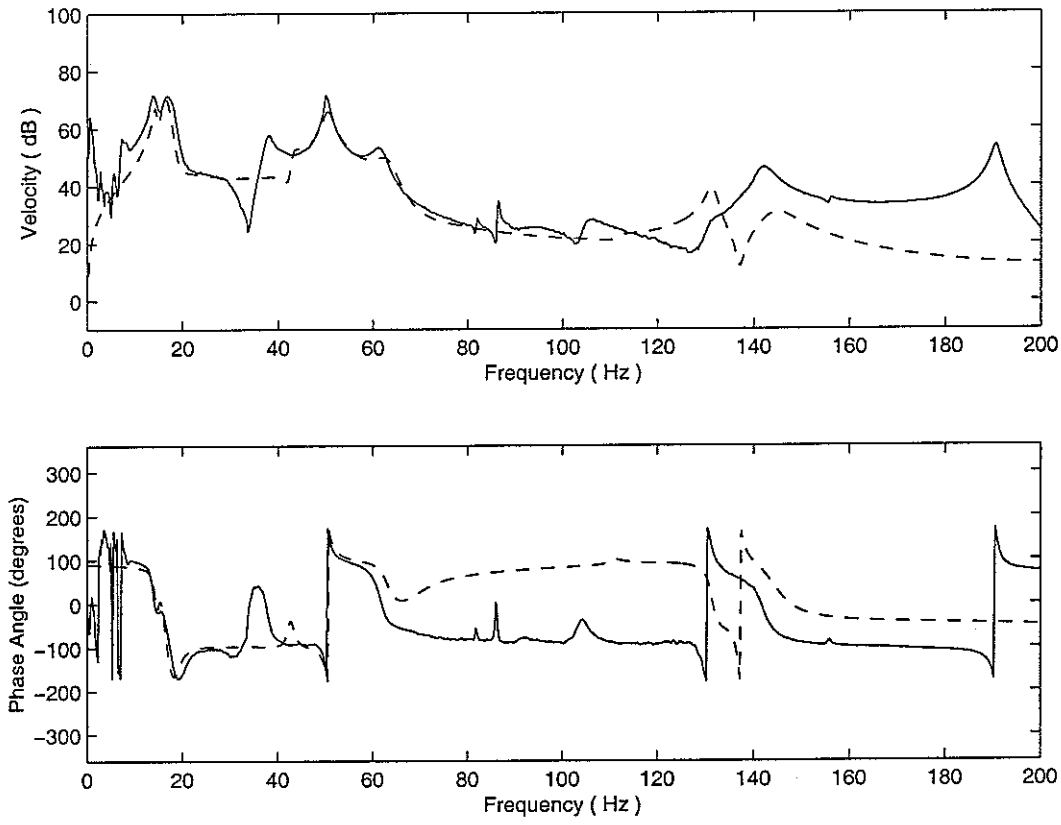

Figure 7 Comparison of plant response G_{14} from simulation (—) and experiment (—)

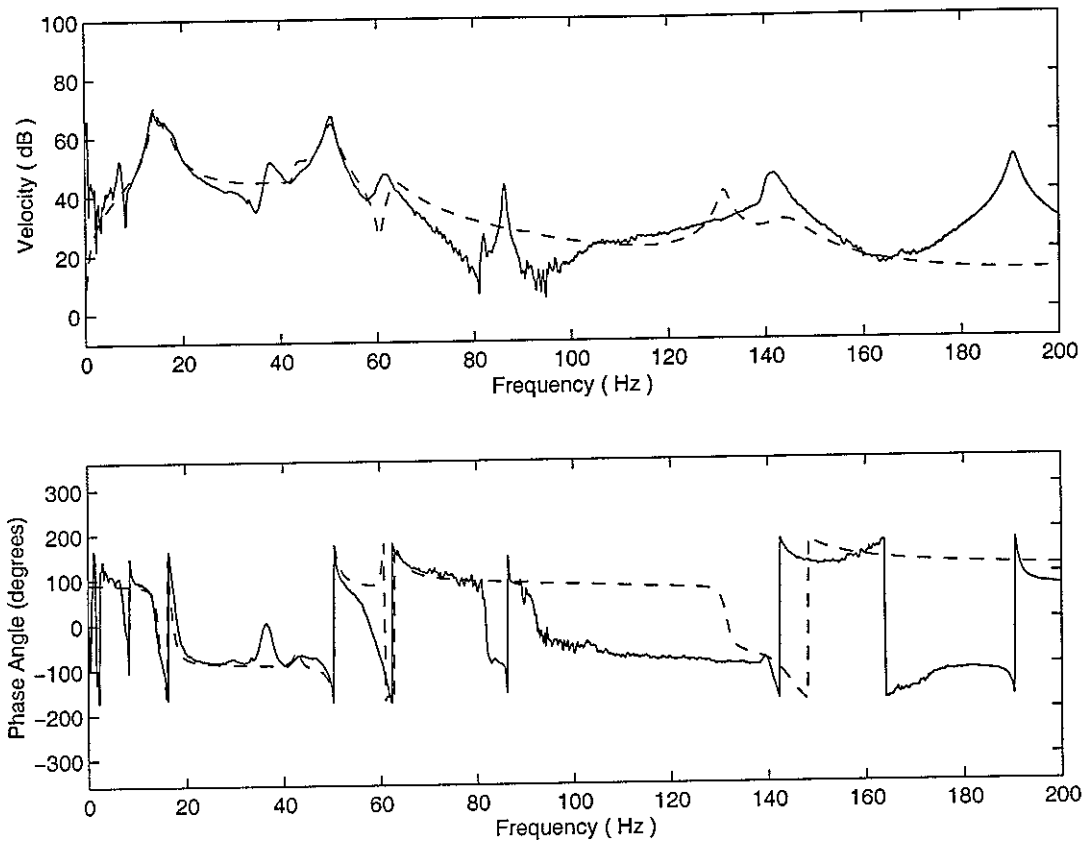

Figure 8 Comparison of plant response G_{21} from simulation (—) and experiment (—)

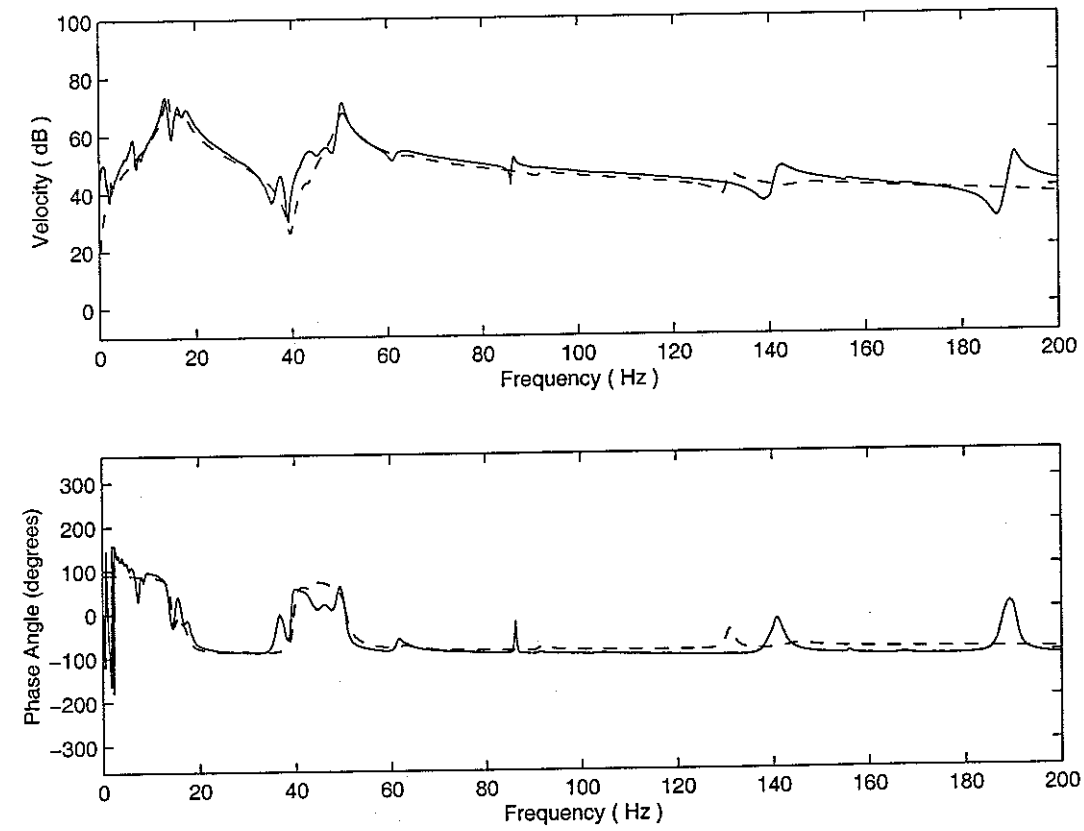

Figure 9 Comparison of plant response G_{22} from simulation (—) and experiment (—)

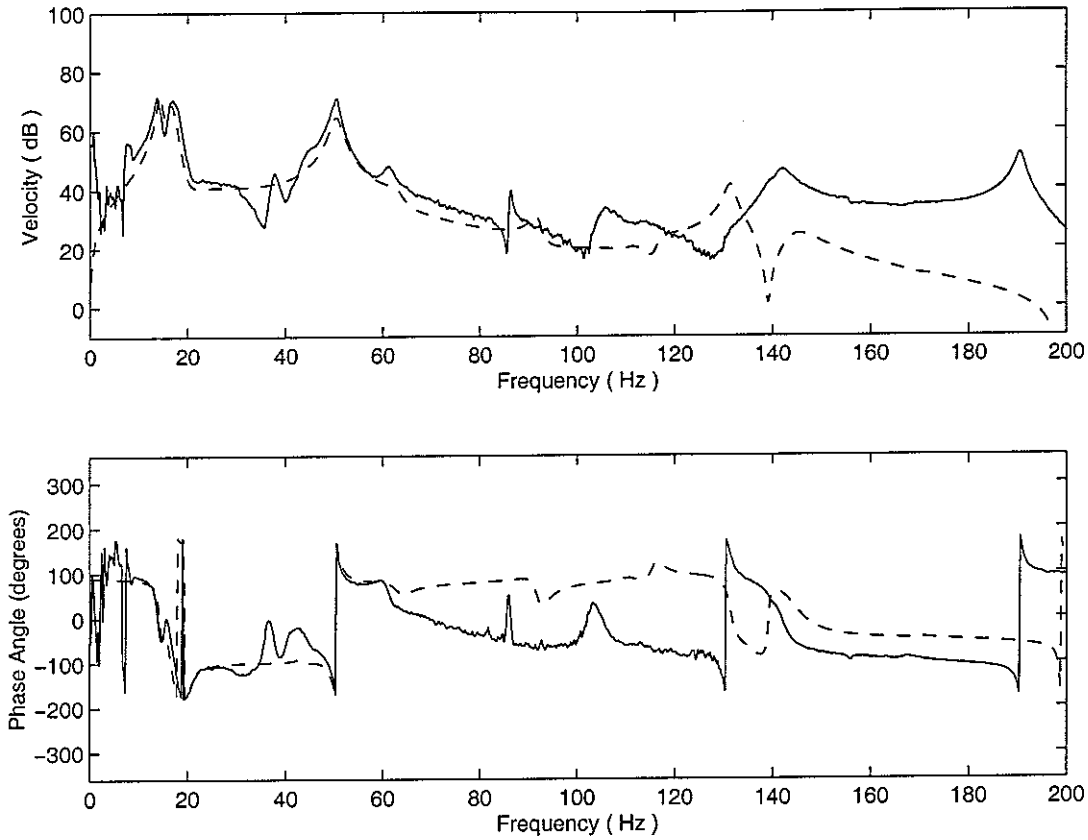

Figure 10 Comparison of plant response G_{23} from simulation (—) and experiment (—)

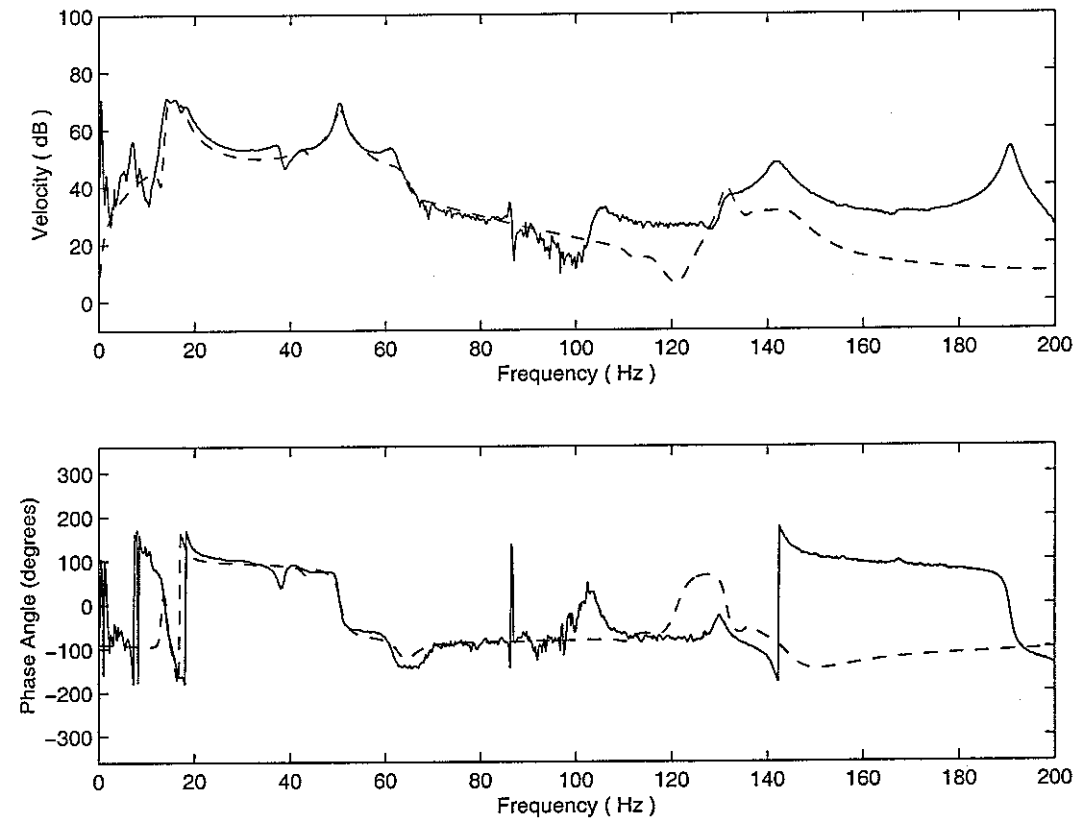

Figure 11 Comparison of plant response G_{24} from simulation (—) and experiment (—)

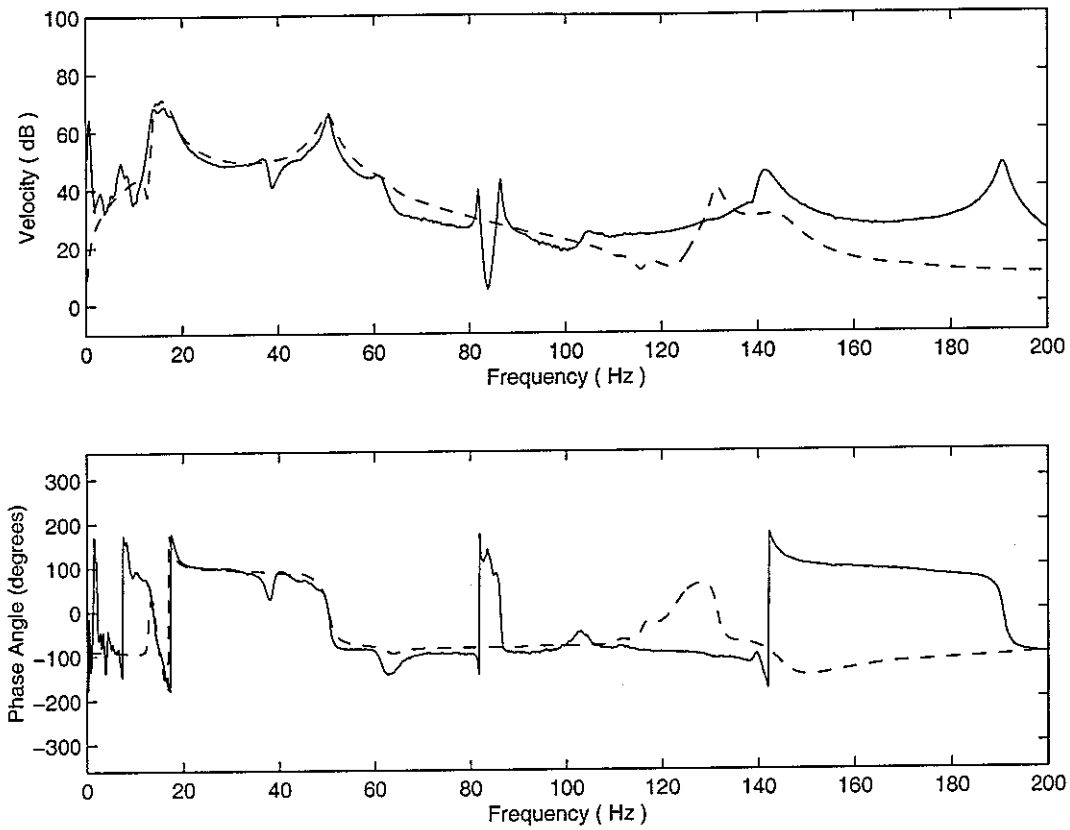

Figure 12 Comparison of plant response G_{31} from simulation (—) and experiment (—)

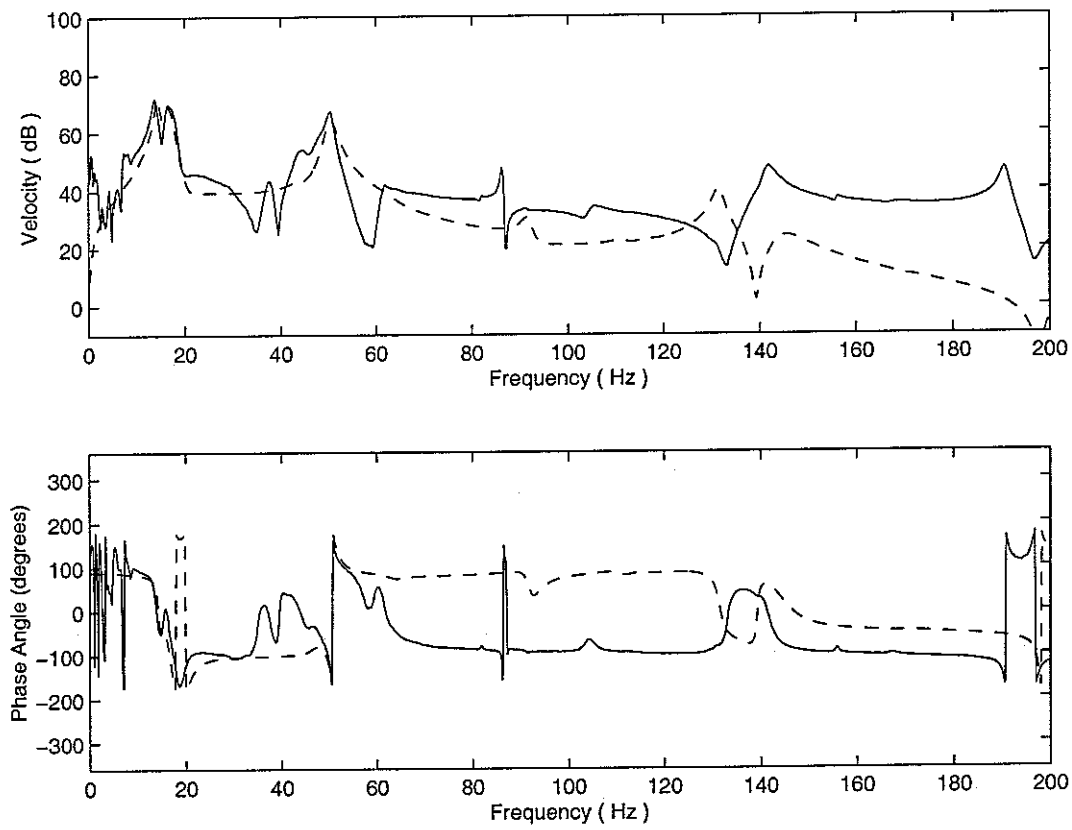

Figure 13 Comparison of plant response G_{32} from simulation (—) and experiment (—)

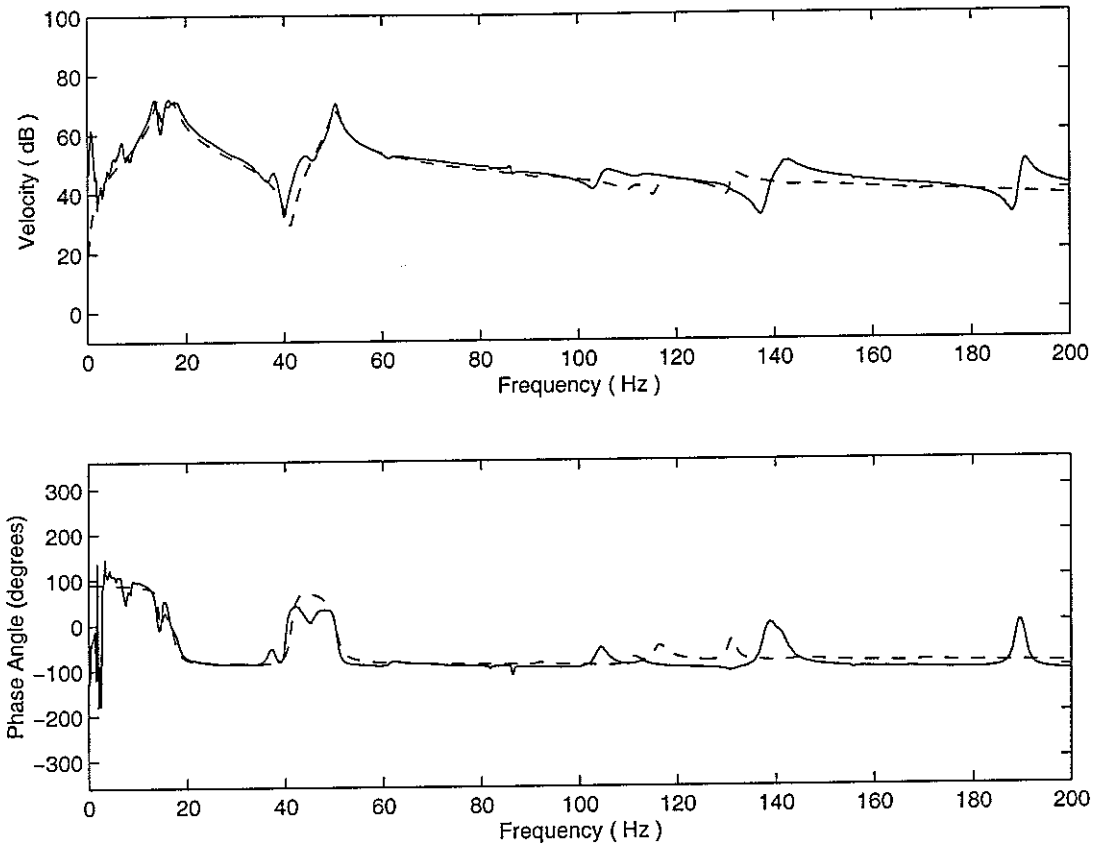

Figure 14 Comparison of plant response G_{33} from simulation (---) and experiment (—)

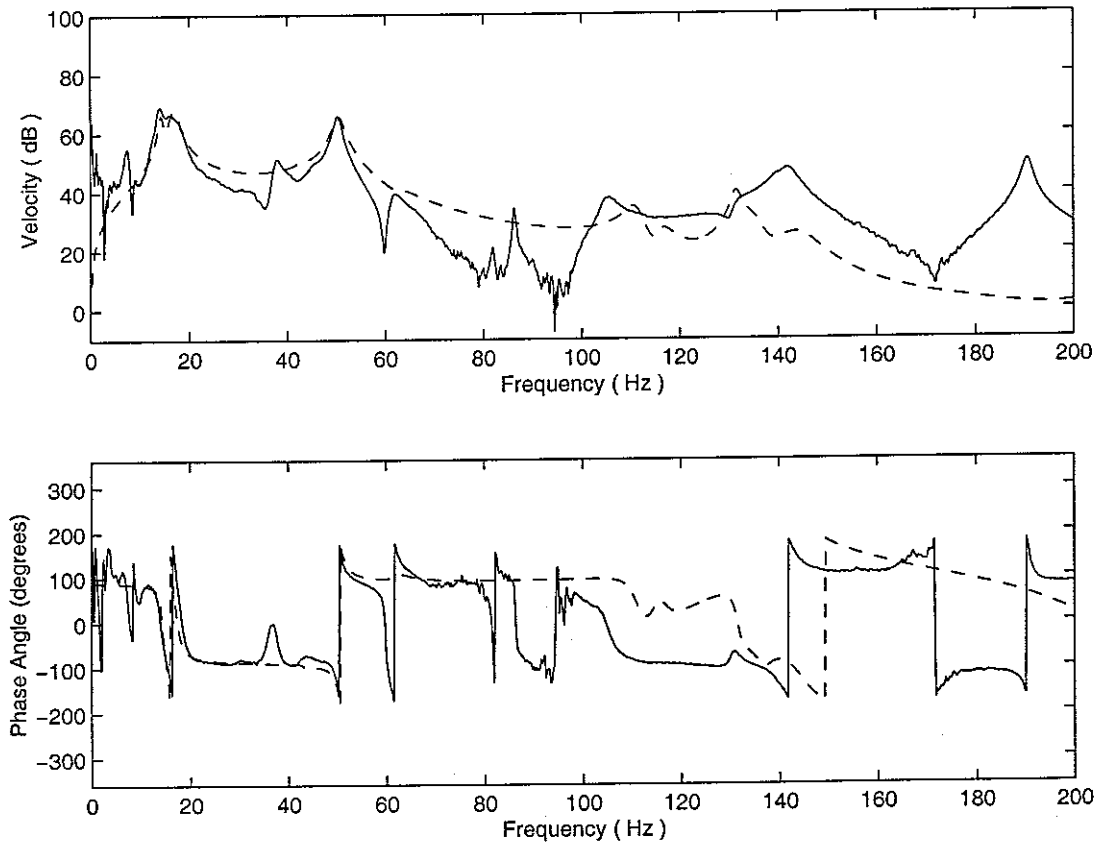

Figure 15 Comparison of plant response G_{34} from simulation (---) and experiment (—)

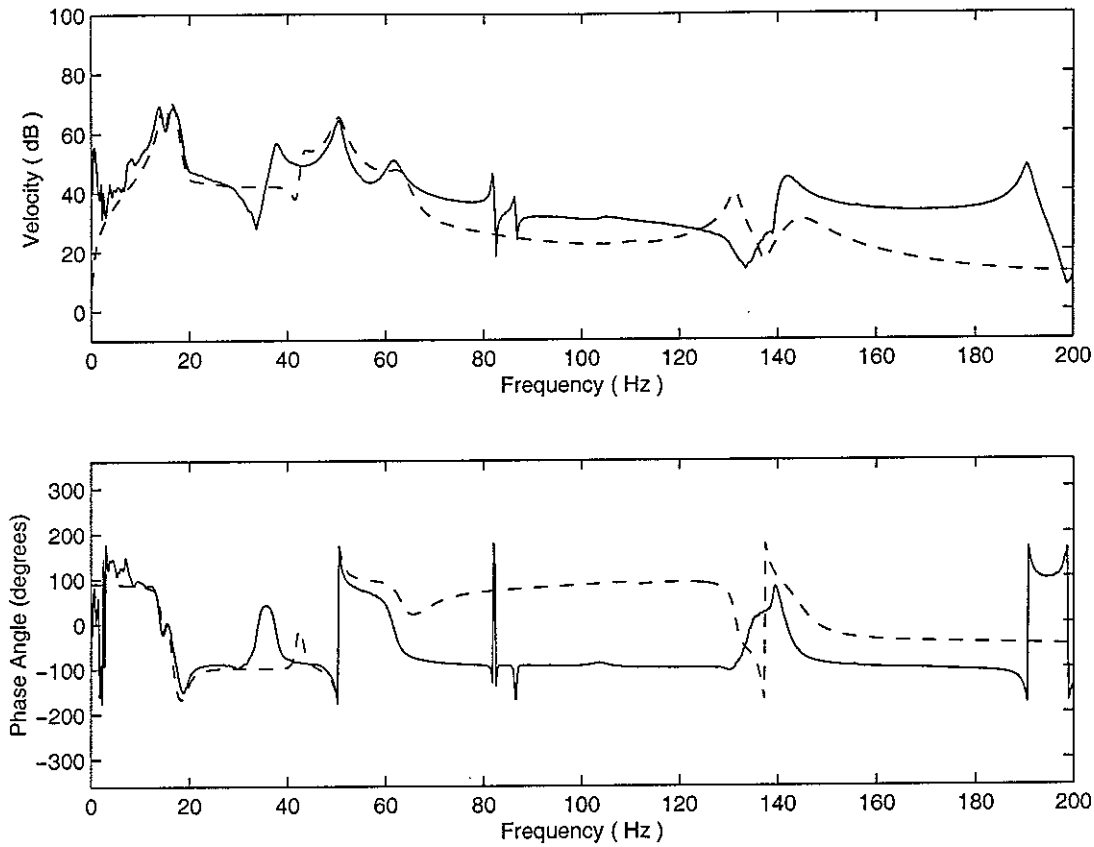

Figure 16 Comparison of plant response G_{41} from simulation (—) and experiment (—)

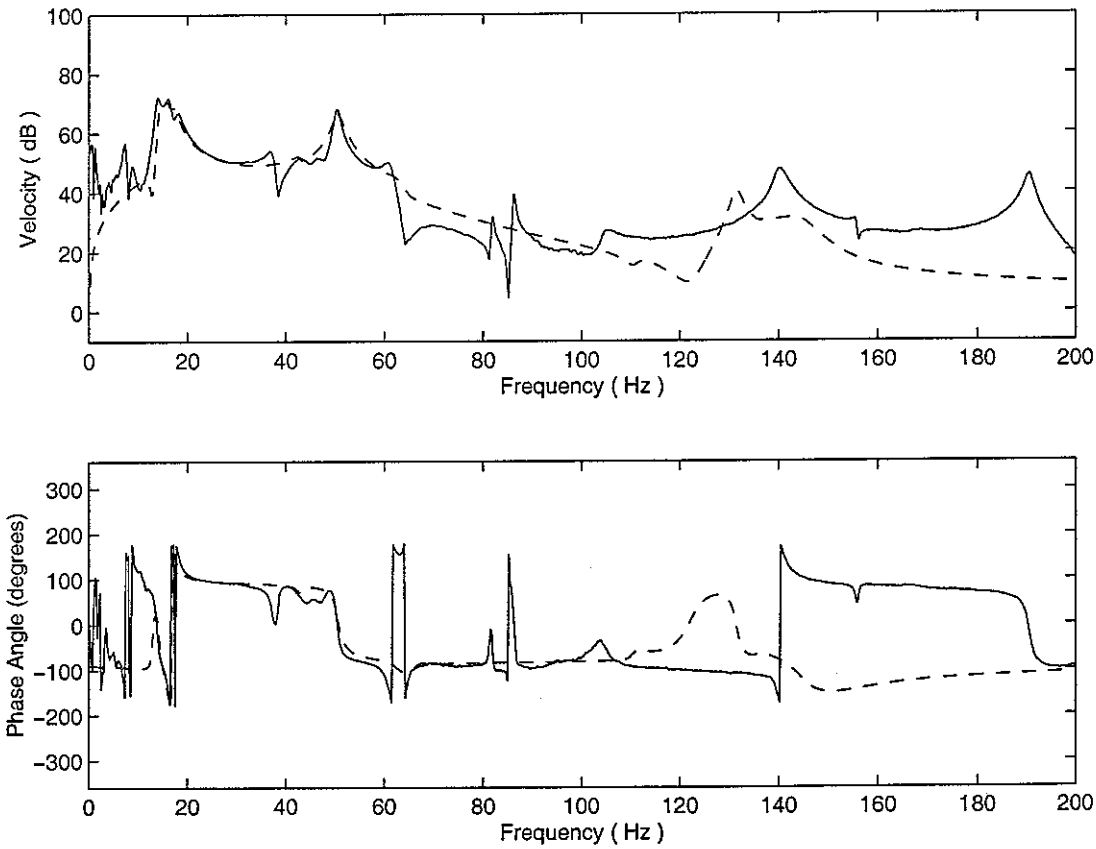

Figure 17 Comparison of plant response G_{42} from simulation (—) and experiment (—)

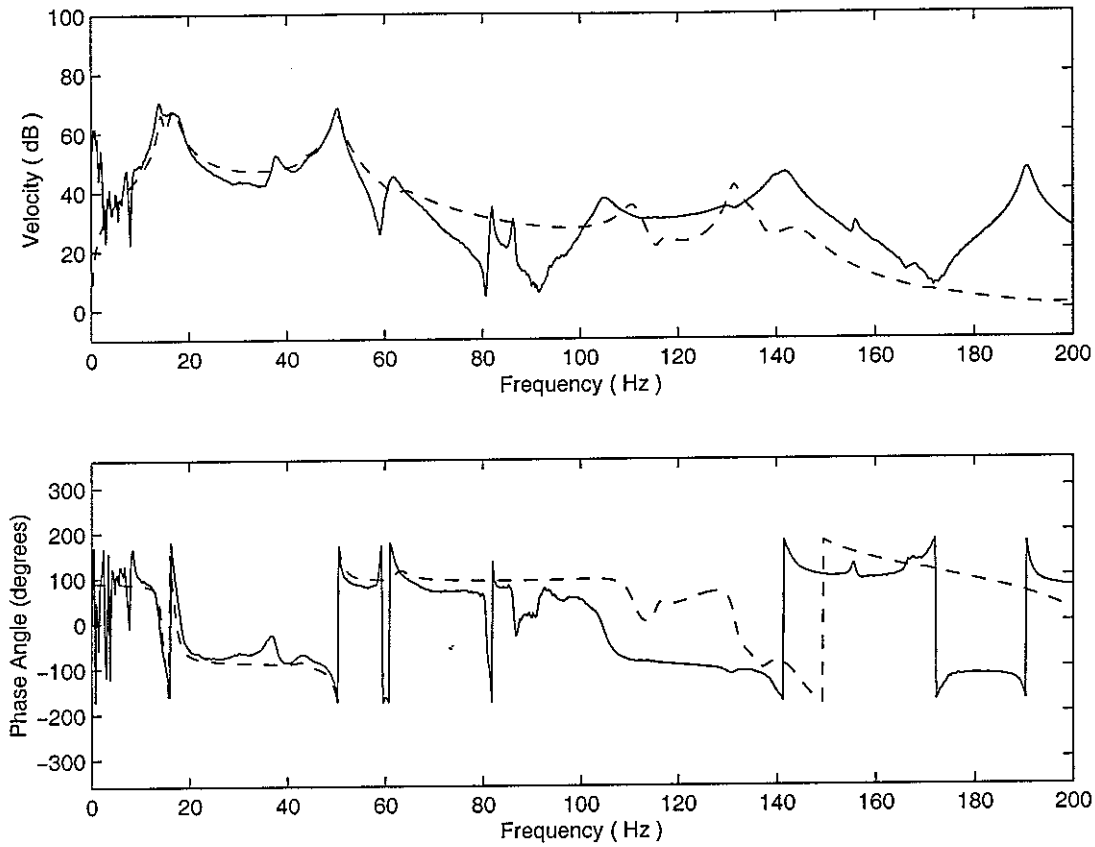

Figure 18 Comparison of plant response G_{43} from simulation (—) and experiment (—)

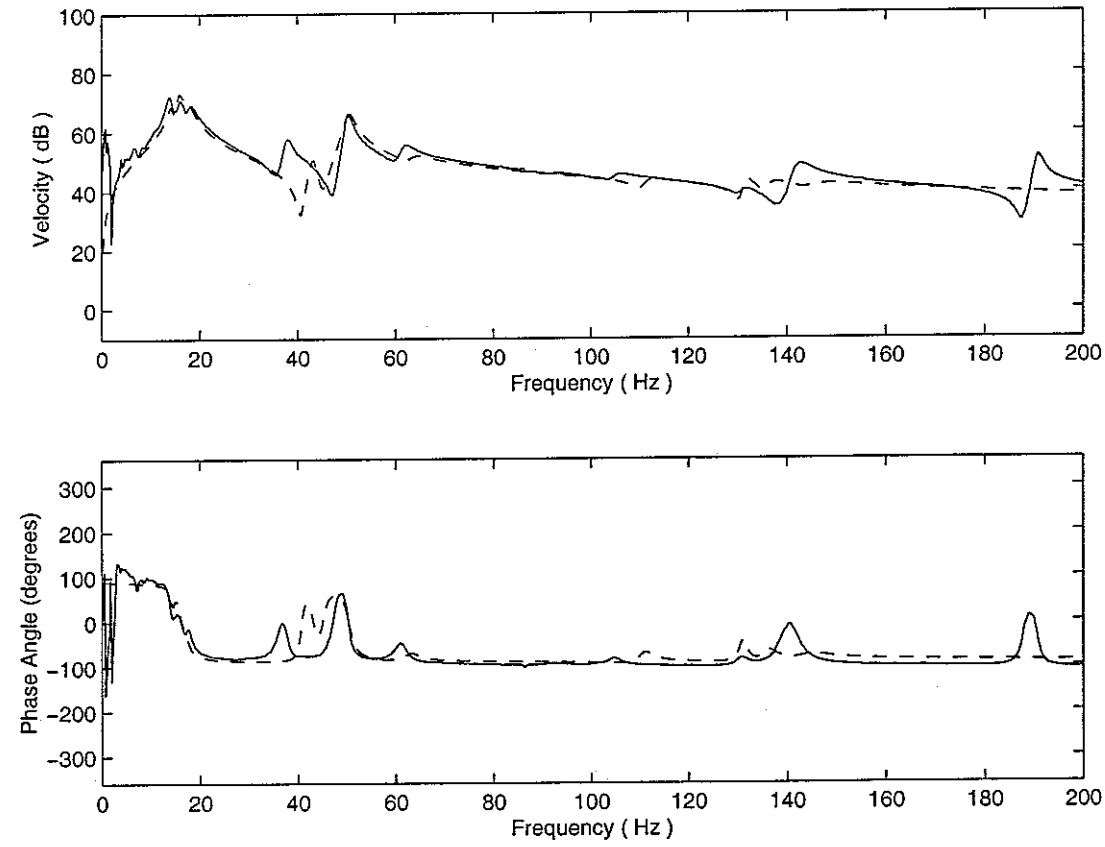

Figure 19 Comparison of plant response G_{44} from simulation (—) and experiment (—)

6 Control stability evaluation

A general electrical block diagram of a multichannel feedback control system as shown in Figure 20 can be used to represent the velocity feedback control system of the mounted equipment structure, which is described by,

$$\mathbf{v}_e = [\mathbf{I} + \mathbf{G}(j\omega)\,\mathbf{H}(j\omega)]^{-1}\mathbf{d} \tag{6}$$

where $\mathbf{I}$ is the identity matrix, $\mathbf{V}_e$ is the equipment velocity vector after control, $\mathbf{d}$ is the vector of primary disturbances which is the velocity responses of the equipment structure without control.

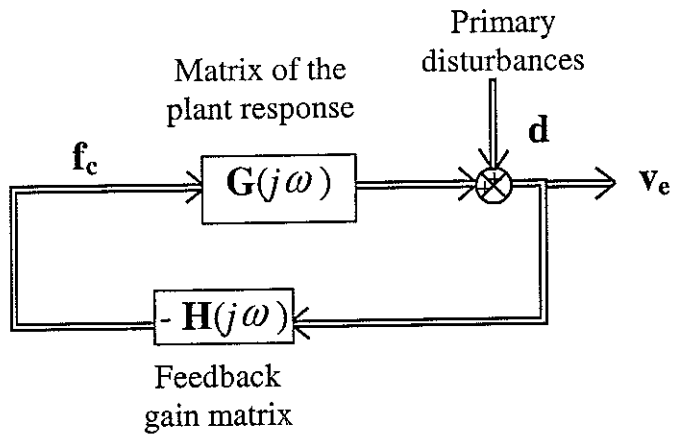

Figure 20 Equivalent electrical block diagram for a velocity feedback control system

Stability of a multichannel velocity feedback control system can be determined from the open loop frequency response function, $\mathbf{L}(j\omega) = \mathbf{G}(j\omega)\mathbf{H}(j\omega)$, using the generalised Nyquist criterion [6]. The closed loop control system is stable provided none of the eigenvalue loci of $\mathbf{L}(j\omega)$ encircles the $(-1, 0)$ point in the complex plane. A decentralised feedback control strategy is employed in this work, which has the advantage of being very simple to implement practically with the complexity rising linearly with the number of channels instead of the square of the number of channels in a fully coupled controller. When an identical constant feedback gain of H is used in each channel, the feedback gain matrix is simply given by,

$$\mathbf{H}(j\omega) = \mathbf{H} = \begin{bmatrix} H & 0 & 0 & 0 \\ 0 & H & 0 & 0 \\ 0 & 0 & H & 0 \\ 0 & 0 & 0 & H \end{bmatrix} \tag{7}$$

Therefore, $\mathbf{L}(j\omega)$ can be rewritten as

$$\mathbf{L}(j\omega) = H\,\mathbf{G}(j\omega) \tag{8}$$

The stability analysis of the four-mount flexible equipment structure is thus simplified to study the Nyquist plots of the eigenvalues of the velocity response matrix $\mathbf{G}(j\omega)$.

The active vibration isolation system is stable if none of the eigenvalue loci of $\mathbf{G}(j\omega)$ encircles the (-1,0) point. If none of the eigenvalue loci crosses the negative real axis, the system is unconditional stable.

For the four-mount flexible equipment structure, the plant response matrix $\mathbf{G}(j\omega)$ of size (4x4) has four frequency dependent eigenvalues. Stability of the multichannel velocity feedback control of the mounted flexible equipment structure on a flexible base structure can thus be assessed on the corresponding Nyquist plots of each eigenvalue loci. An inherent numerical difficulty in obtaining the eigenvalue as a smooth function of frequency generally arises within MALAB, however, an algorithm has been developed to sort the eigenvalues, which is described in detail in reference [4].

Prior to assessing the stability of the multichannel control system, it is useful to evaluate the stability of a single channel controller. When the flexible base structure is excited by the primary shaker, a single channel control can be implemented by feeding back the equipment velocity at one of the four mount positions to the corresponding actuator. For the special case of a single channel velocity feedback control system using a constant gain at the ith mount position, the stability can be assessed by examining the Nyquist plot of the corresponding diagonal velocity response term, $G_{ii}(j\omega)$. Therefore, Nyquist plots of the diagonal terms of the plant response matrix, $G(j\omega)$, from both simulation and experiment are compared in Figures 21 to 24.

For the single channel velocity feedback control, the active vibration isolation system exhibits very good stability properties from both simulation and experiment, since almost the whole Nyquist plot of the corresponding diagonal plant response term, $G_{ii}(j\omega)$, lies in the right real half plane. The large loops are related to the rigid body modes of the mounted equipment structure, which appeared in the Bode plots of plant responses in the previous section. The flexible modes of the active vibration isolation system is characterised by several small loops, whose radii decrease as the passive mounts become more efficient with increasing frequency. As perfect operation of the electrical equipment in the control loop is assumed in the simulation, the Nyquist plots of the diagonal plant responses from the simulation are totally in the positive real half plane. Most of the Nyquist plots of experimental results lies in the stable right half plane, except for a very small region at very low frequencies suffered from the low sensitivities of the actuators and sensors. At low frequencies, the highpass filter and integrator inside the charge amplifier may cause additional phase shifts, which tends to be $\pi/2$. This is not expected to cause instability, but will give rise to vibration amplification at very low frequencies. The phase shift has to be added to the phase shift of the power amplifier at low frequencies. Theoretically, a phase advance of a little over 90° at low frequencies is sufficient for the Nyquist plot to cross the negative real axis. Thus, the phase shifts at very low frequencies are the causes of the small responses noticed on the upper left side of the origin in the Nyquist plots of the diagonal plant responses obtained from the experiment. However, these effects are not large since the absolute value of the phase is never significantly larger than $\pi/2$, and are always associated with small amplitude vibrations. The measured plant responses do not have a strictly positive real part in the frequency band of analysis, which indicates that the actuators are not strictly collocated with the sensors for the

installation of the active vibration isolation system due to the flexibility of the equipment structure being isolated. In practice, the diagonal plant elements are almost entirely positive real above about 10 Hz, indicating that there is not a significantly different vibration response between the experimental actuators and sensors. Therefore, main threat to the single channel control stability comes from the phase shifts of the electrical devices used in the experiment if the feedback control gain is very large.

Stability of the four-channel control system of the mounted flexible equipment structure on a flexible base is also assessed using the Nyquist criterion in terms of the eigenvalue loci. The amplitudes and corresponding phase angles of the eigenvalues were calculated and shown in Figures 25 to 28 (dB ref.=10^{-5}). The predicted results match reasonably well with the experimental results, which further validates the theoretical model developed for the active vibration isolation system. The Nyquist plots of the eigenvalue loci from the simulation (dashed line) and experiment (solid line) were illustrated in Figures 29 to 32. Each plot from the simulation and experiment has one main loop, as each eigenvalue is proportional to a certain mode of the mounted equipment structure. Due to the imperfect operation of the electrical equipment and low coherence suffered at low frequencies, the corresponding plots from the experiment slightly cross the imaginary axis at very low frequencies, although the effect is very small. Smooth curves at low frequencies are observed in the simulation since perfect operation of the electrical equipment is assumed. The loci predicted from the simulation lies wholly within the stable right half plane. However, in practice there are relatively very small loops in the middle of the frequency range as shown in the lower left half plane of the experimental Nyquist plots. The difference between the theory and experiment originates from the fact that the feedback control implemented in the experiment is not a collocated control strictly due to the flexibility of the equipment. As the feedback gain increases, the radii of the small loops in the left half plane of the Nyquist plots of the eigenvalue loci becomes greater and greater. Eventually the multichannel control system of the mounted equipment structure on a flexible base goes unstable, when the eigenvalue loci encircle the (-1,0) point for a large feedback gain. As most of the eigenvalue loci lies in the stable right half plane, however, good stable property of the multichannel control system is expected. The main threats to the control stability come from the phase shifts in the electronics of the control loop at low frequencies as similarly pointed out for the case of single channel control system and non-collocation of the sensors and actuators.

An assumed mode shape method was also employed to study the stability of the multichannel feedback control system for the mounted equipment structure on a rigid base structure [4]. However, the method is only an approximation without strict theoretical proof, and thus is not employed in this report. Figures 33 to 40 are illustrated in this section for information only.

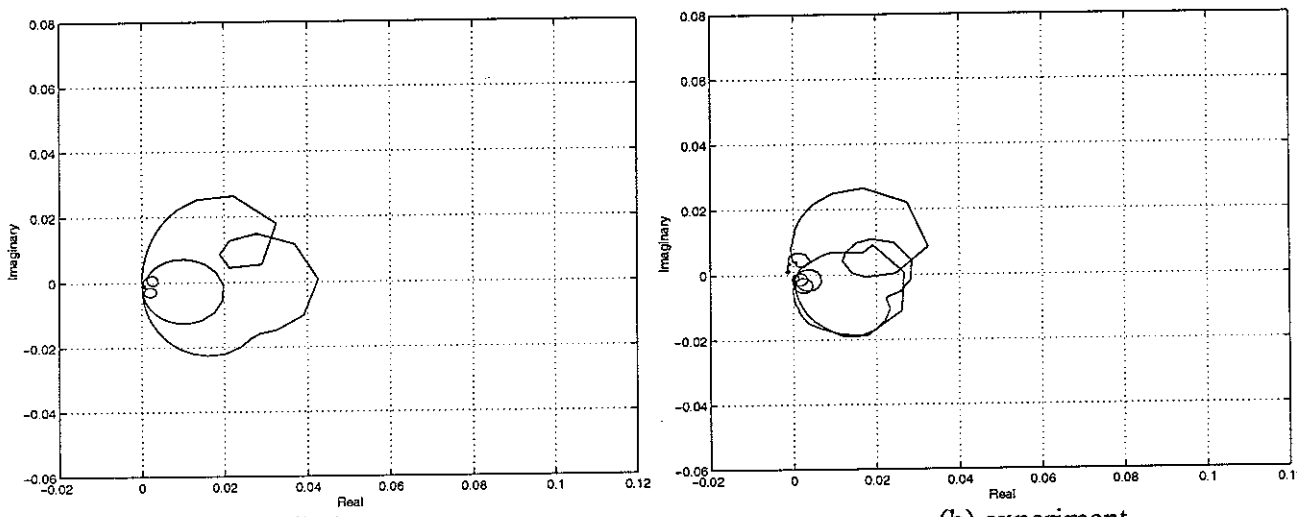

(a) Prediction (b) experiment

Figure 21 Nyquist plot of the plant response G_{11} for a single channel control at node 1

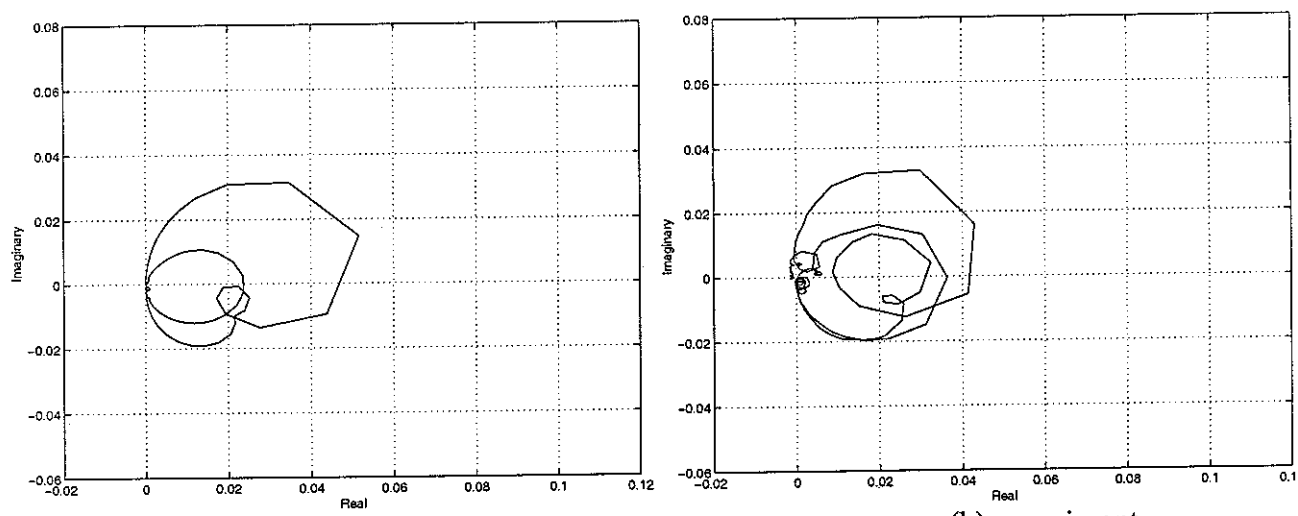

(a) Prediction (b) experiment

Figure 22 Nyquist plot of the plant response G_{22} for a single channel control at node 2

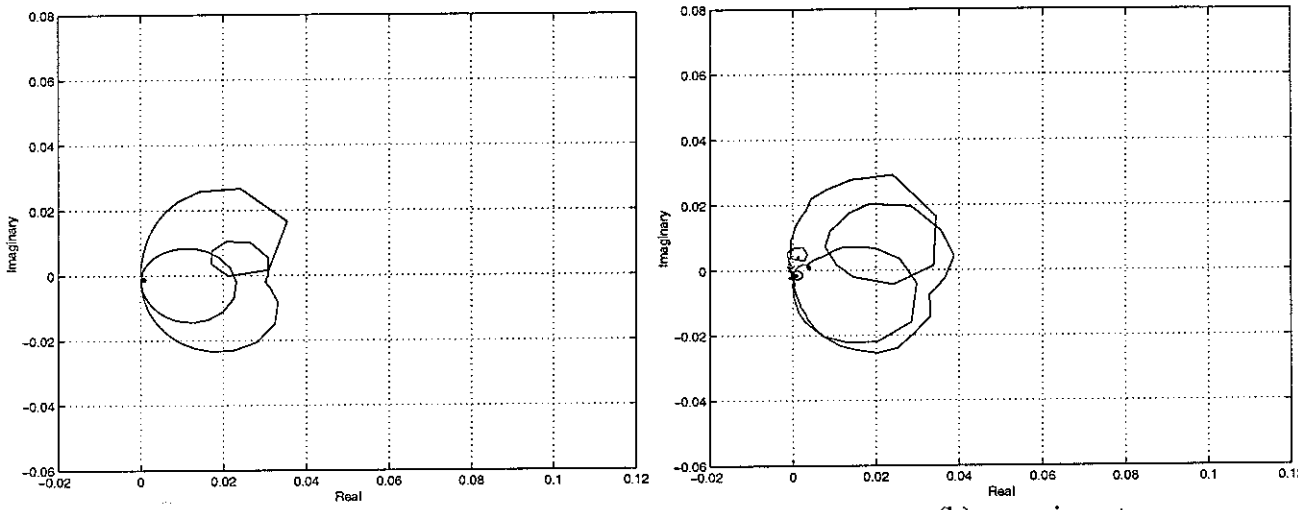

(a) Prediction (b) experiment

Figure 23 Nyquist plot of the plant response G_{33} for a single channel control at node 3

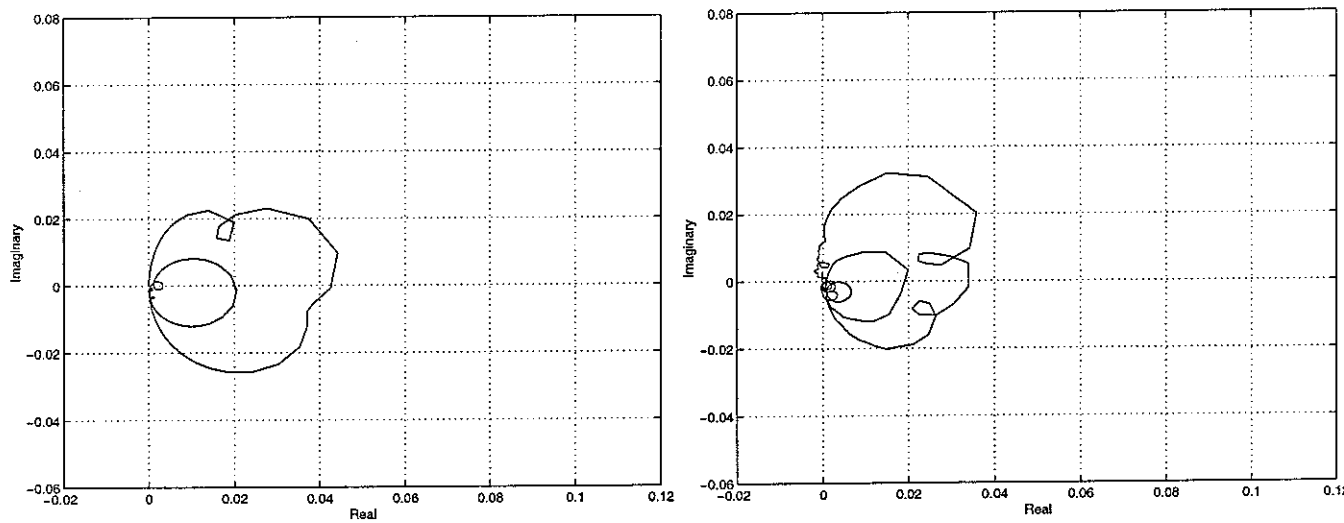

(a) Prediction (b) experiment

Figure 24 Nyquist plot of the plant response G_{44} for a single channel control at node 4

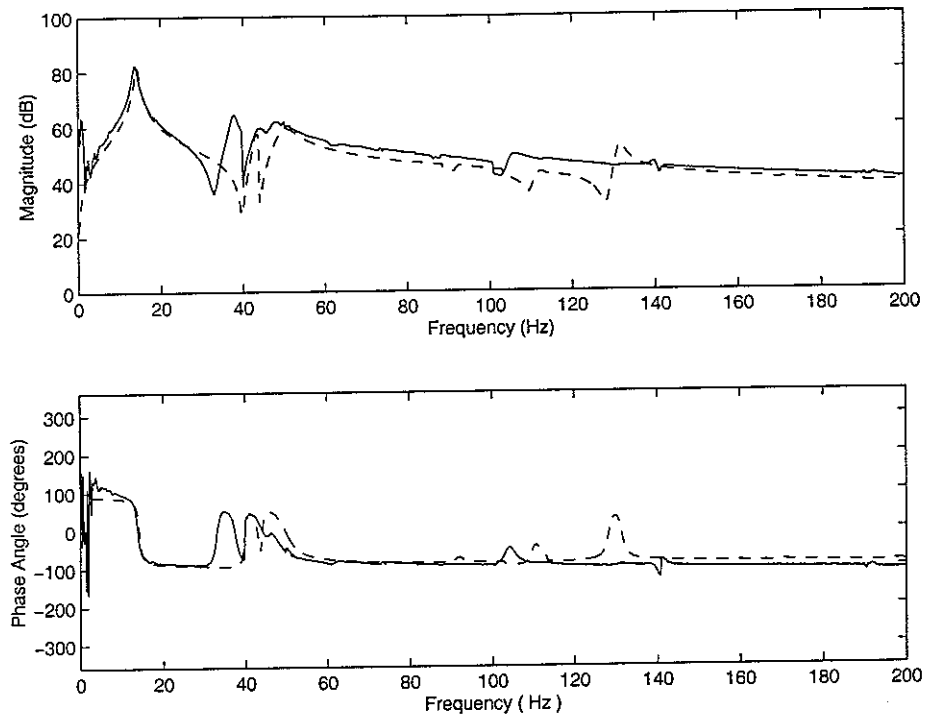

Figure 25 Bode plot of the eigenvalue λ_1 of the mounted equipment structure (simulation: dashed line -- , experiment: solid line —)

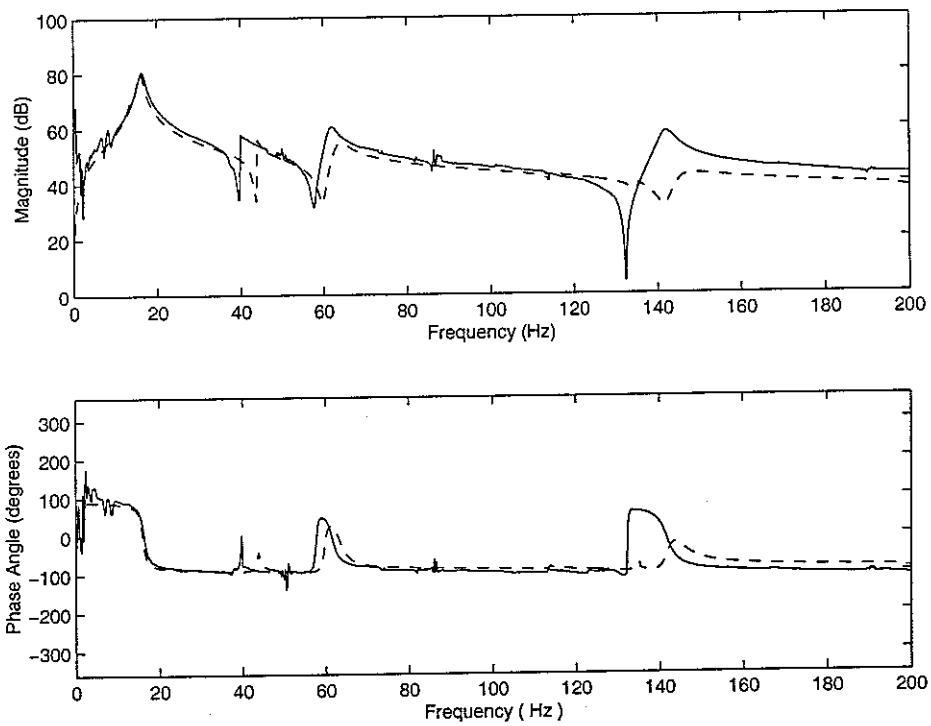

Figure 26 Bode plot of eigenvalue λ_2 of the mounted equipment structure (simulation: dashed line -- , experiment: solid line —)

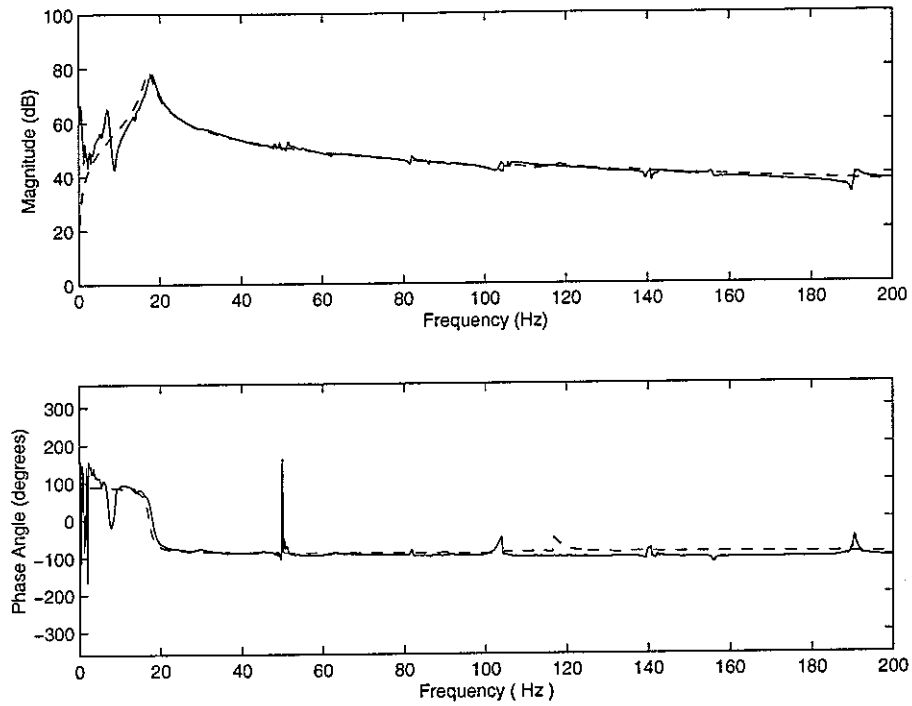

Figure 27 Bode plot of the eigenvalue λ_3 of the mounted equipment structure (simulation: dashed line -- , experiment: solid line —)

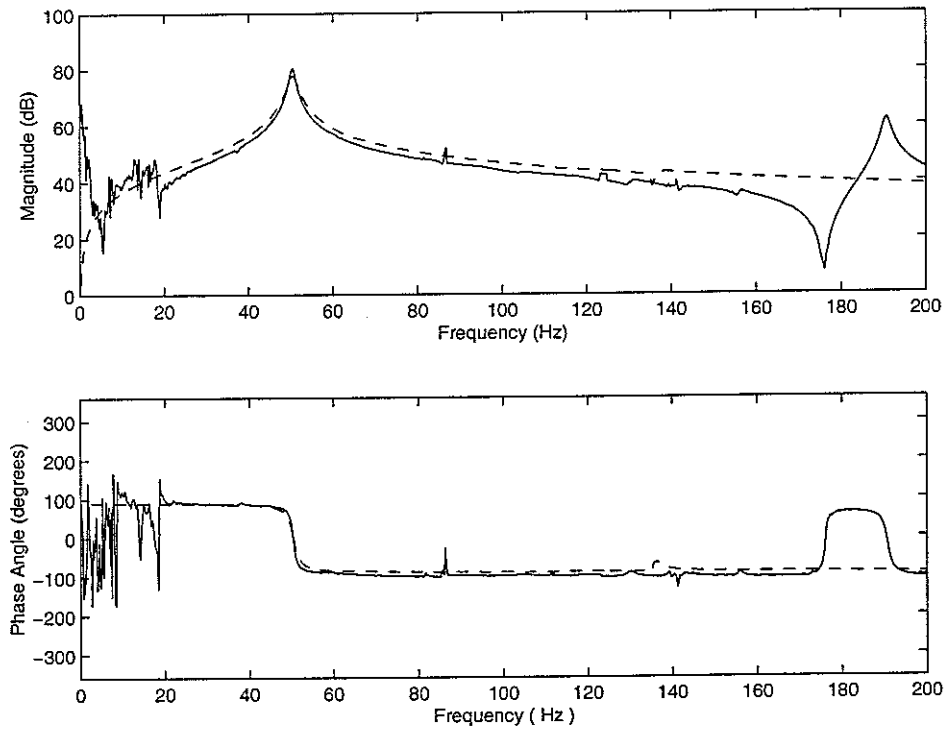

Figure 28 Bode plot of the eigenvalue λ_4 of the mounted equipment structure (simulation: dashed line -- , experiment: solid line —)

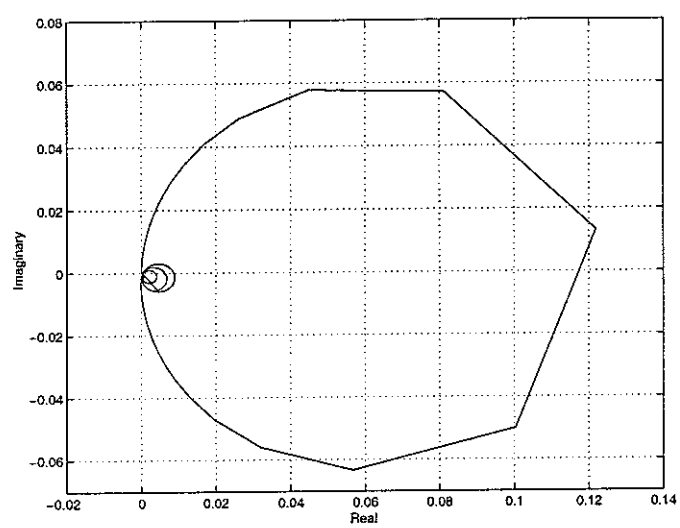

(a) Prediction

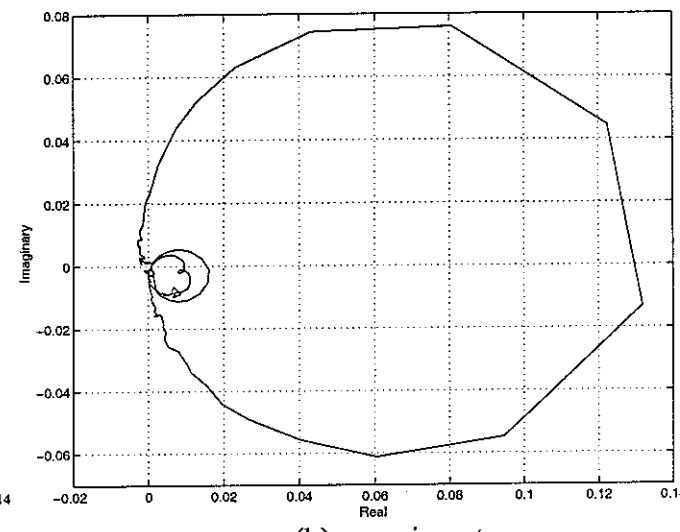

(b) experiment

Figure 29 Nyquist representation of the eigenvalue λ_1

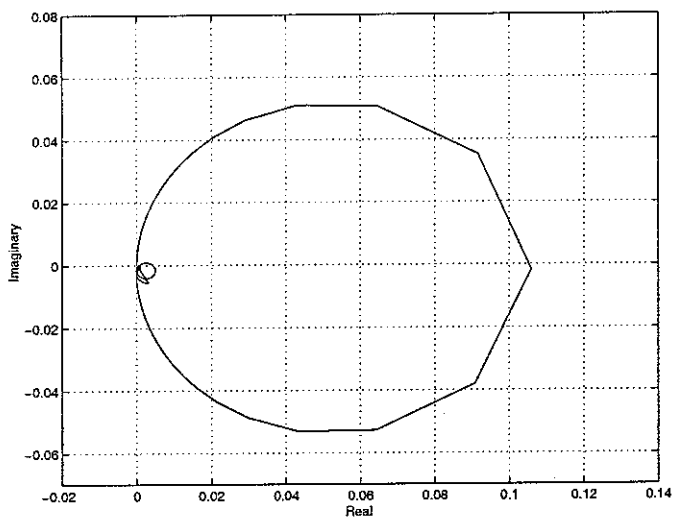

(a) Prediction

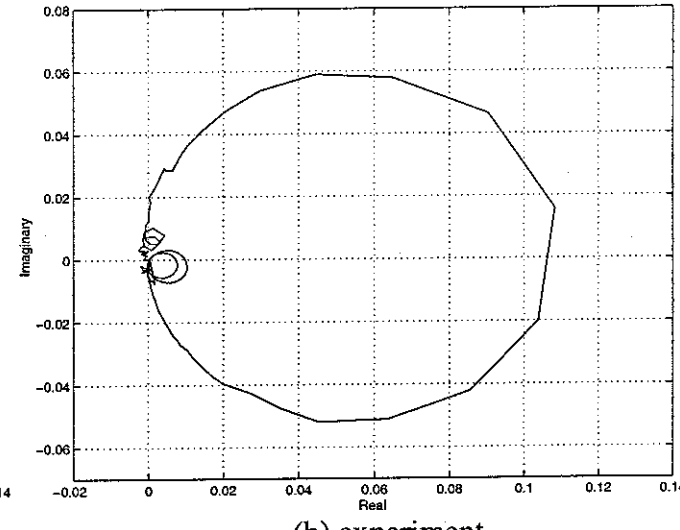

(b) experiment

Figure 30 Nyquist representation of the eigenvalue λ_2

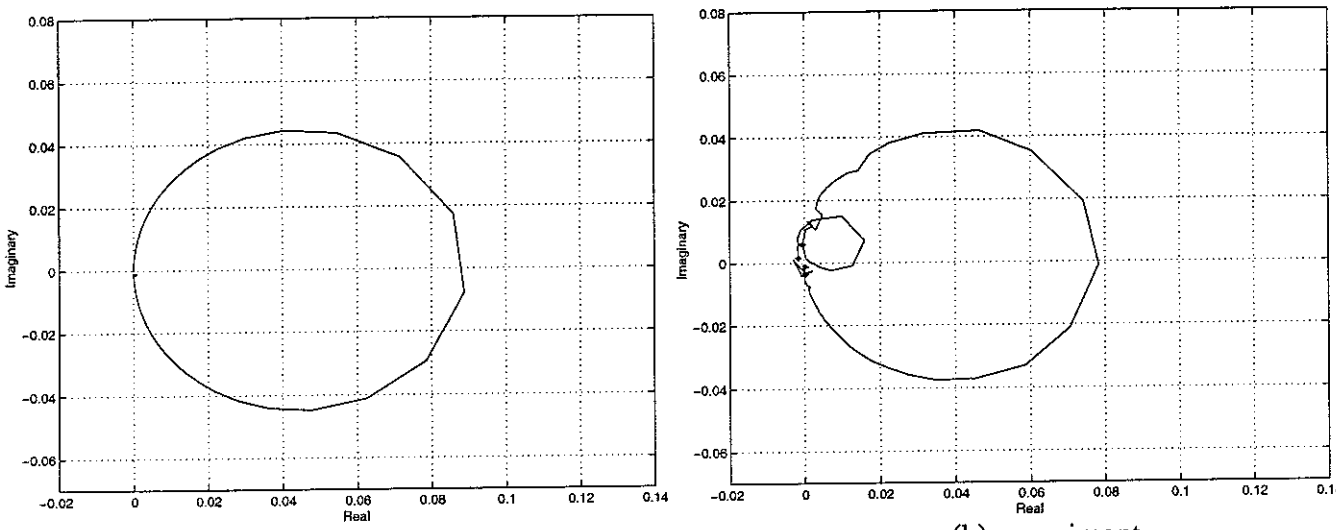

(a) Prediction (b) experiment

Figure 31 Nyquist representation of the eigenvalue λ_3

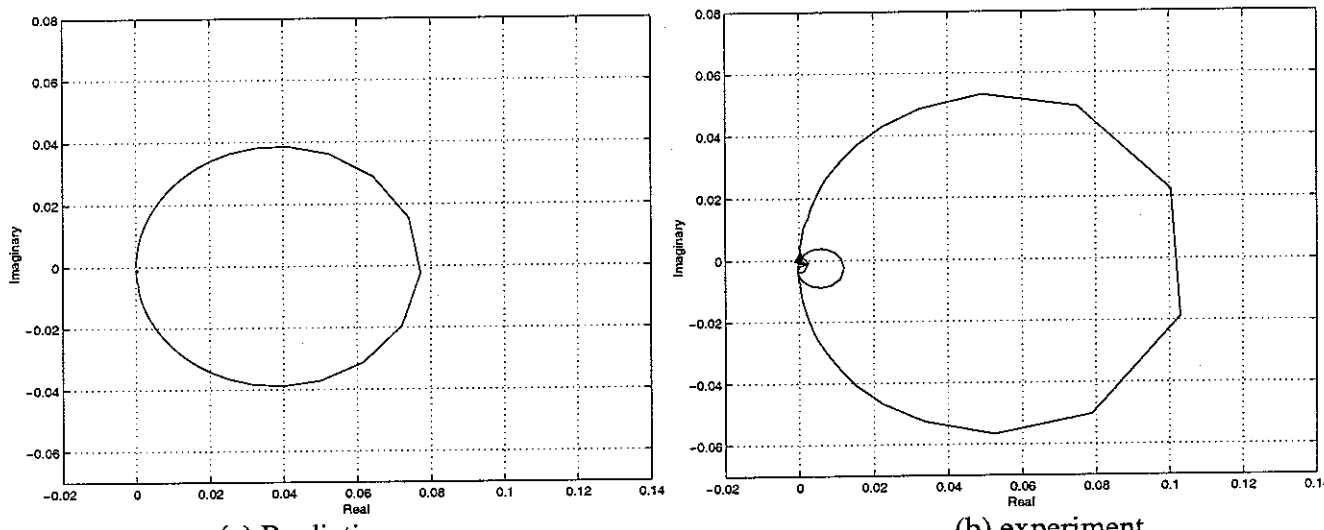

(a) Prediction (b) experiment

Figure 32 Nyquist representation of the eigenvalue λ_4

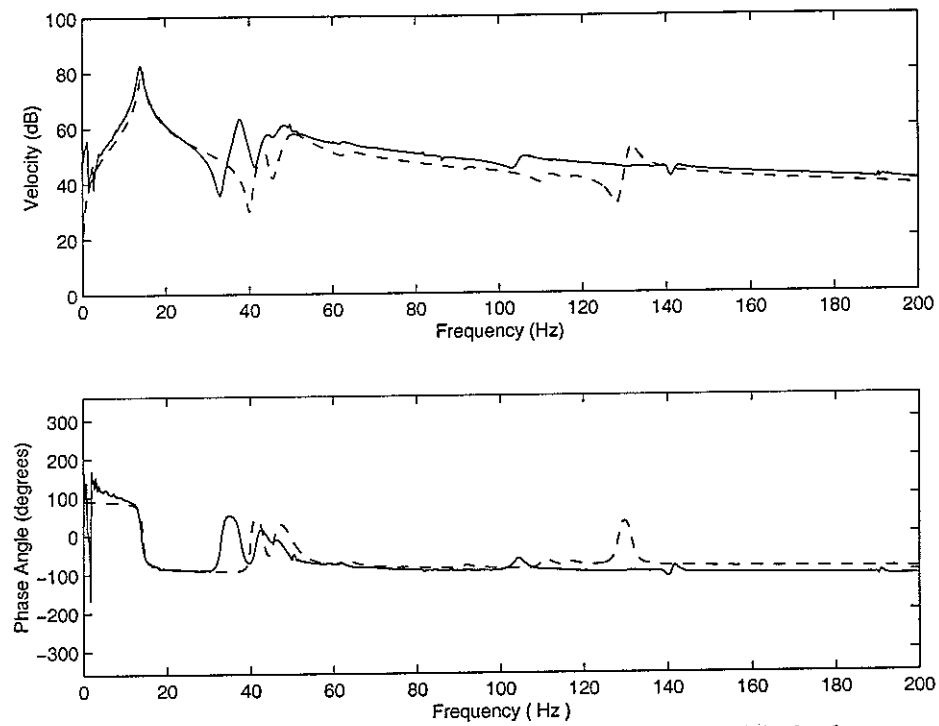

Figure 33 Bode plot of the assumed eigenvalue associated with the heave mode (simulation: dashed line -- , experiment: solid line —)

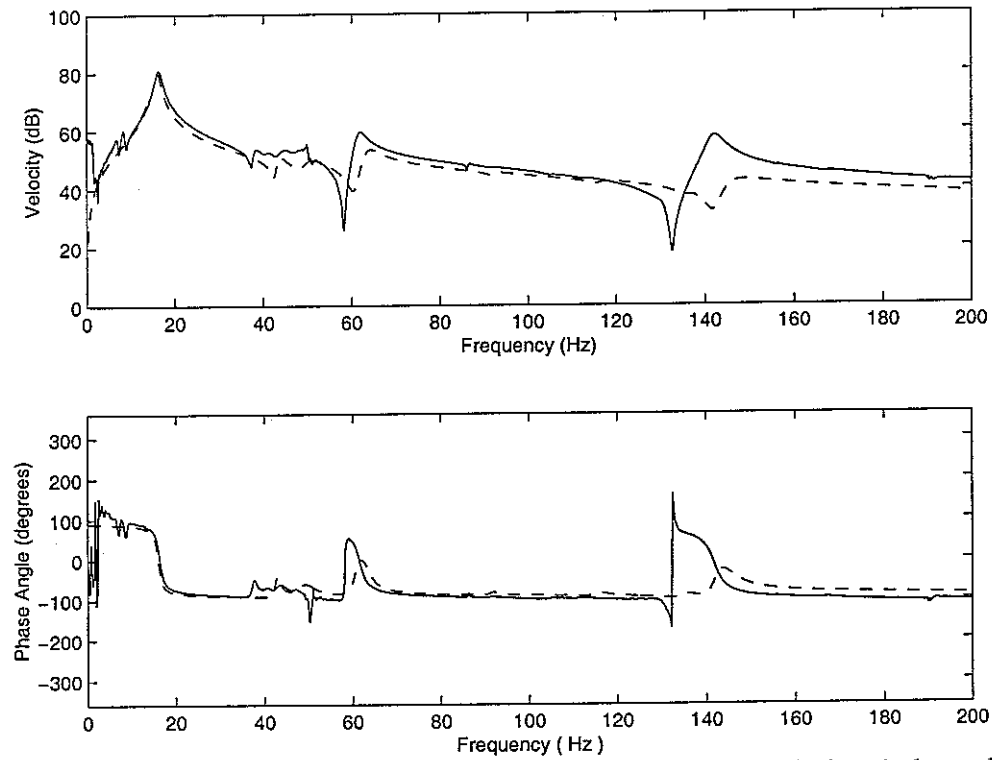

Figure 34 Bode plot of the assumed eigenvalue associated with the pitch mode (simulation: dashed line -- , experiment: solid line —)

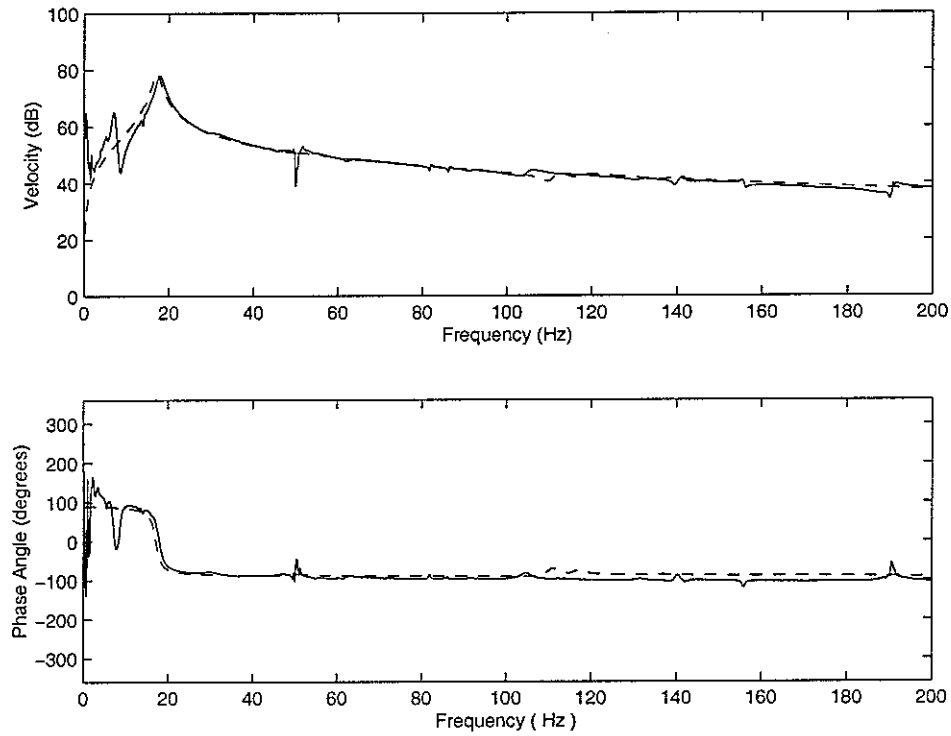

Figure 35 Bode plot of the assumed eigenvalue associated with the roll mode (simulation: dashed line -- , experiment: solid line —)

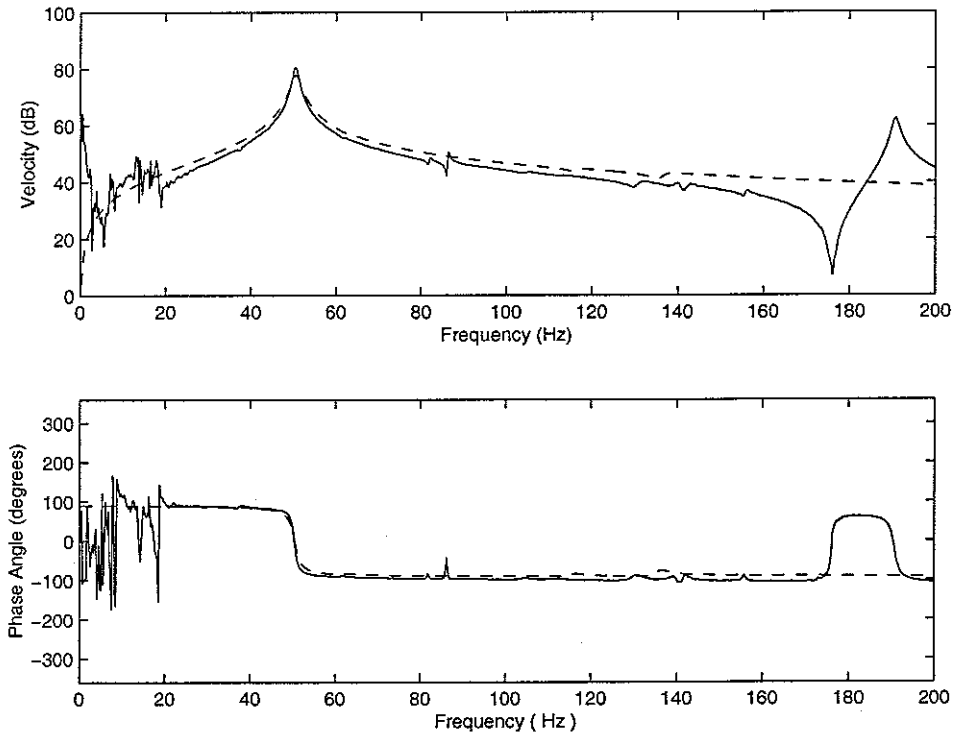

Figure 36 Bode plot of the assumed eigenvalue associated with the torsion mode (simulation: dashed line -- , experiment: solid line —)

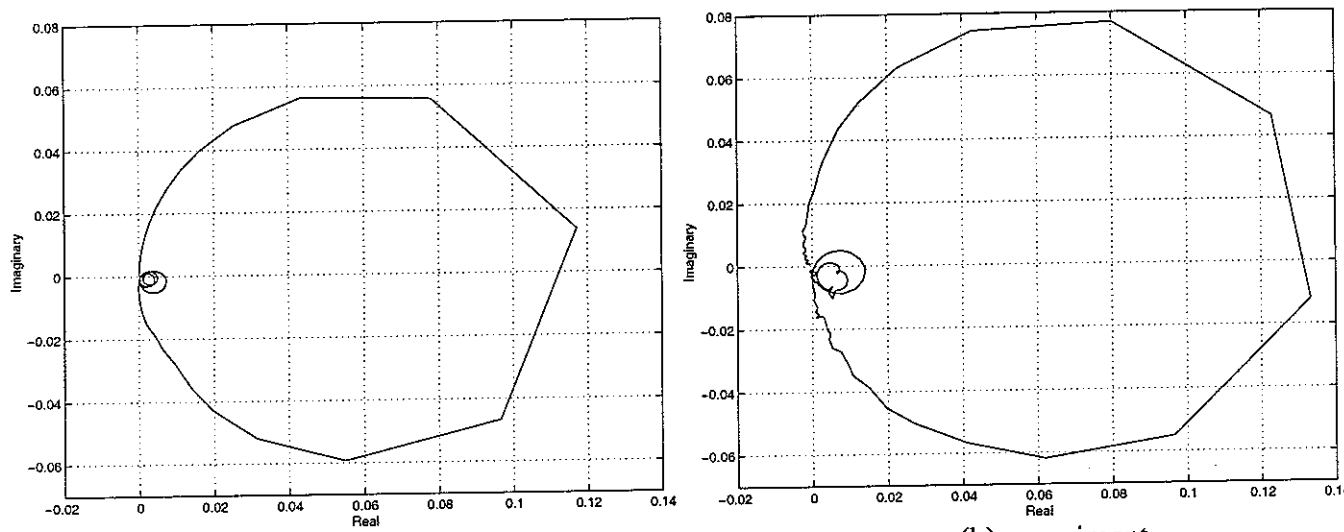

(a) Prediction (b) experiment

Figure 37 Nyquist representation of the assumed eigenvalue loci associated with the heave motion

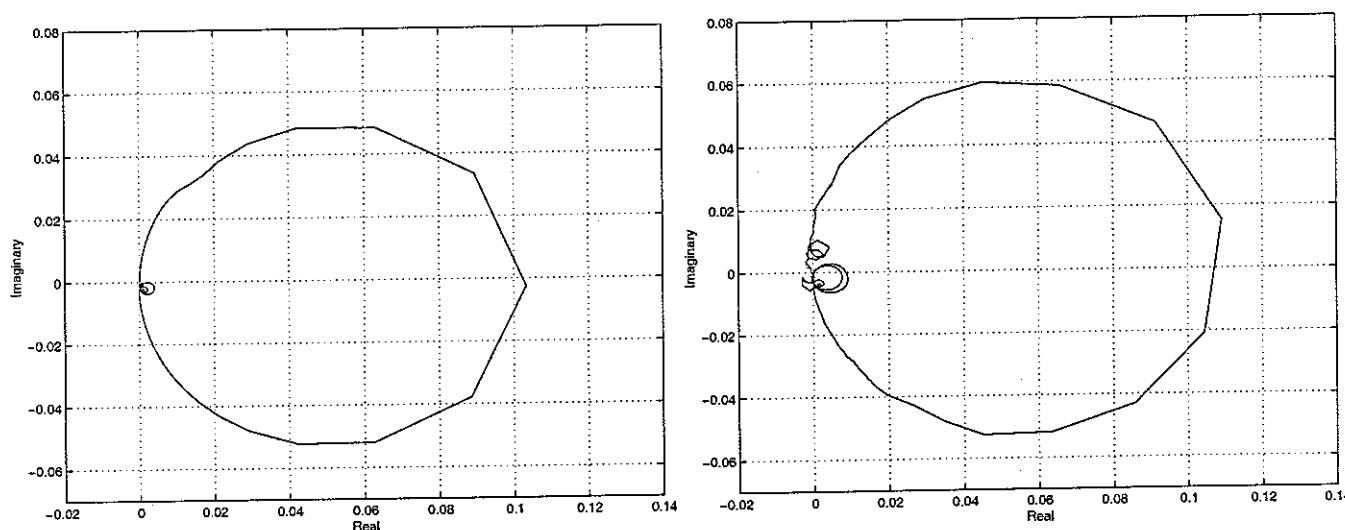

(a) Prediction (b) experiment

Figure 38 Nyquist representation of the assumed eigenvalue loci associated with the pitch motion

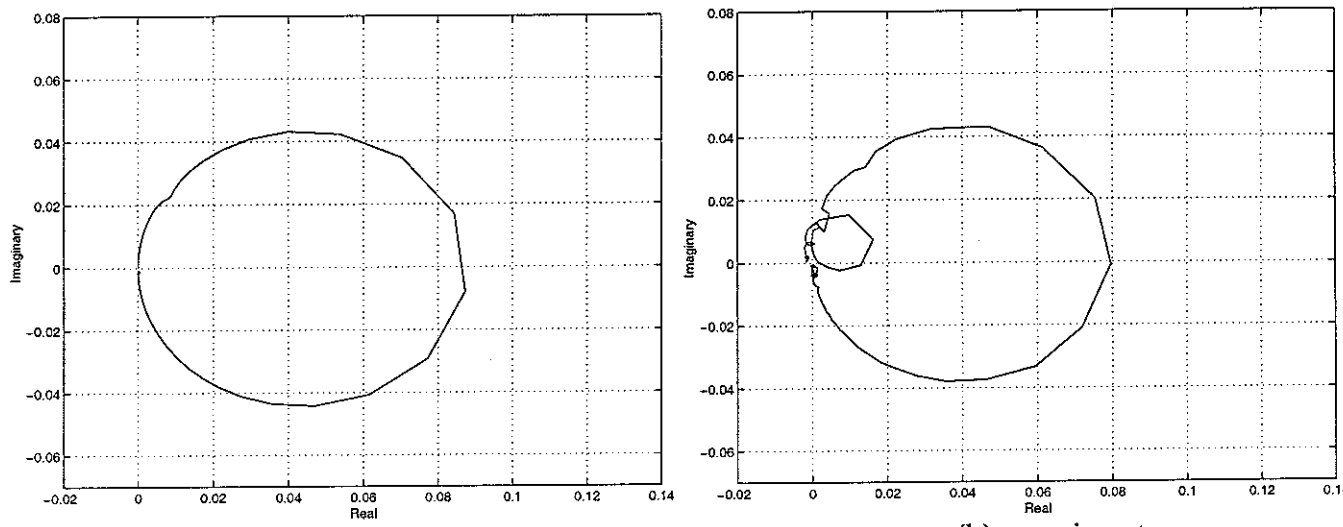

(a) Prediction (b) experiment

Figure 39 Nyquist representation of the assumed eigenvalue loci associated with the roll motion

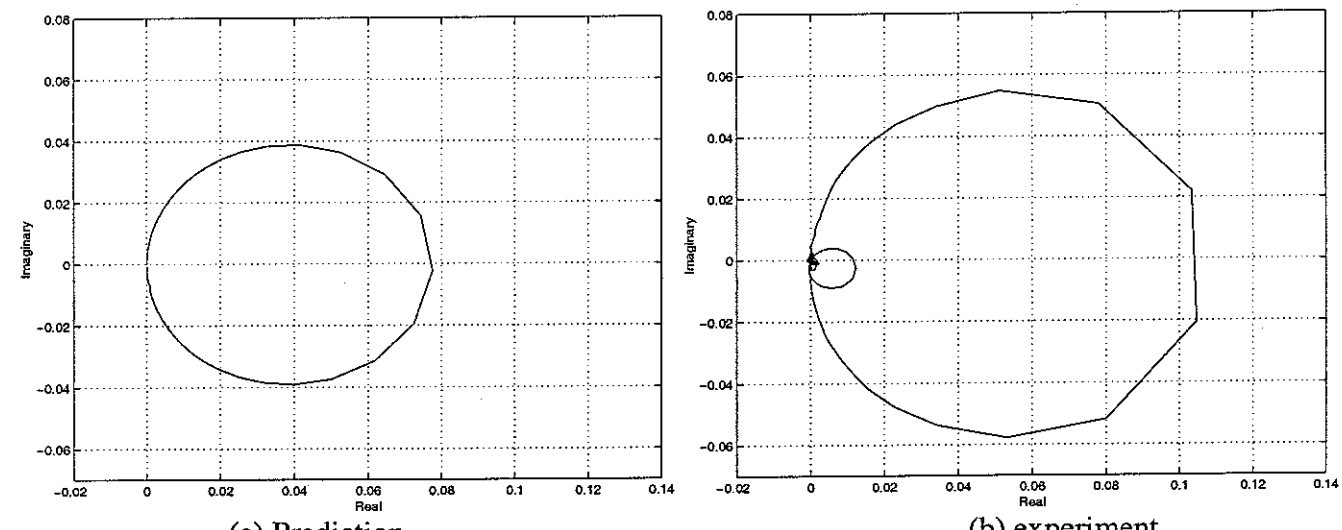

(a) Prediction (b) experiment

Figure 40 Nyquist representation of the assumed eigenvalue loci associated with the torsion motion

7 Control performance

7.1 Single channel velocity feedback control implementation

In this section, a single-input-single-output (SISO) control is implemented at one of the four mount positions for the active vibration isolation system prior to implementing the four-channel decentralised velocity feedback control. The aim is to assess the extent to which the equipment structure could be isolated from a vibrating base with only a single controller. The practical configuration of the single channel velocity control system is illustrated in Figure 41.

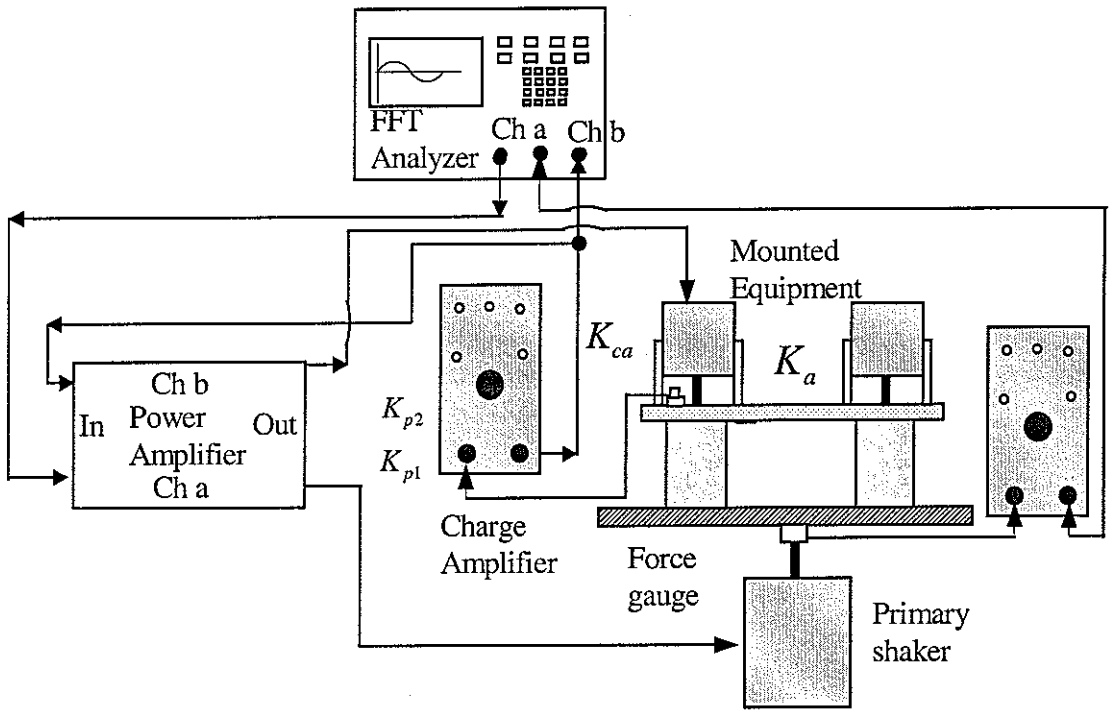

Figure 41 Practical configuration of a single channel control system

Typical velocity responses at the control position of mount 1, as well as at the non-controlled mount position 2, 3 and 4 are shown in Figures 42 to 45 (dB ref.=10^{-5} m/s). The velocity responses before control (dashed line) and after control (solid line) are compared to investigate the control performance both theoretically and experimentally. In the simulation, the feedback control gain relating the secondary force to the control velocity in unit of Ns/m must account for the different gains used in the experimental feedback loop, which comprises the charge amplifier gain K_{ca}, the power amplifier gain K_{p2}, and the sensitivity of the actuator K_a (equal to 0.91 Nv^{-1}). The sensitivity of the accelerometer is directly taken into account by the charge amplifier. Therefore, the feedback control gain can be calculated by,

$$H = K_a K_{p2} K_{ca} \tag{9}$$

When setting the sensor sensitivity properly, the charge amplifier has a gain of 100 mv per ms^{-1}. Multiple control gains are then applied through the power amplifier in order to have a parametric demonstration of control performance. The gain values from the power amplifier were measured and equal to 2, 10 and 22 in the experiments. Therefore, feedback control gain values of 0.182, 0.910 and 2.002 Ns/m were calculated from equation (36) and modelled in the simulation for comparison purposes. Higher feedback control gains of up to 11.83 Ns/m may be applied in the experiment for this configuration of a single channel controller before instability occurs, which corresponds to a gain of 13 from the power amplifier and a gain of 1000 mv per ms^{-2} from the charge amplifier. A gain margin of approximately 15 dB is then obtained for a SISO control system with a flexible equipment structure in practice.

It is clearly demonstrated in Figure 42 that the vibration levels at the control point are effectively reduced at all the resonance frequencies of the coupled system both theoretically and experimentally. The theoretical predictions are in good agreement with the experimental results. In particular, up to 20 dB reductions at the rigid body modes, as well as up to 15 dB attenuation at the first flexible mode (50.5 Hz) of the mounted equipment structure, have been achieved at the control point when single channel control is implemented. The vibration levels of the equipment structure at the base plate resonances are also attenuated at the direct controlled point by up to 4 dB at around 38 Hz and 6 dB at around 62 Hz in practice. With the passive isolation performance increasing, the control effect of a single channel feedback controller decreases and only small reductions in vibration are observed at other higher resonance frequencies. Generally, the effect of the velocity feedback control gradually decreases with increasing frequency, since the control force is proportional to the control velocity, which is strongly attenuated by the passive mount at high frequencies. In the experiment, the vibration level at very low frequencies is actually amplified due to the phase shift. Similar conclusions can be made from Figures 46 to 48 where the single channel control is implemented at node 2, 3 and 4 respectively. The control performances at non-directly controlled point are different from these at directly controlled points as seen from Figures 43 to 45, where the velocity responses at node 2, 3 and 4 are shown when the single channel feedback control is implemented at node 1. The vibration levels at non-directly controlled points are attenuated at the resonance frequencies of the mounted equipment structure by a smaller extent compared to the attenuations obtained at the direct controlled points. However, amplifications of the vibration are generally obtained at several resonance frequencies of the base structure, as clearly seen in Figure 44 at about 40 Hz both theoretically and experimentally.

In summary, a SISO velocity feedback control of the four-mount flexible equipment structure was investigated both theoretically and experimentally in this section. Considerable reductions in the vibration level at the direct controlled positions were achieved at all resonance frequencies both in the experiments and simulations. At the non-directly controlled points, small attenuations less than 10 dB could be still achieved at the resonance frequencies of the mounted equipment structure, although amplifications of vibration level were generally observed at some of the base plate resonance frequencies. In addition, the phase shifts due to the imperfect operation of the electrical equipment in the experiments, induced amplifications of vibration level at very low frequencies (less than 5 Hz) in practice.

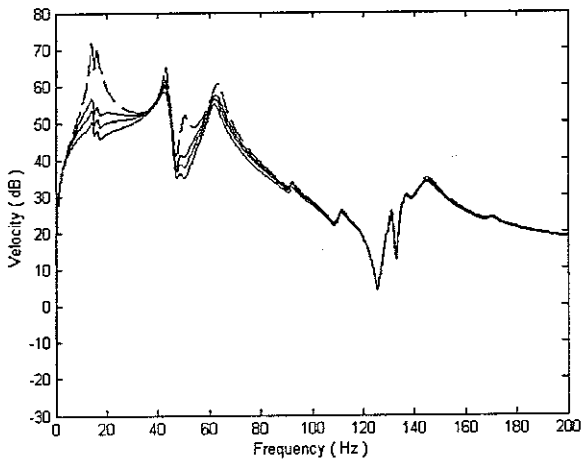

(a) Prediction

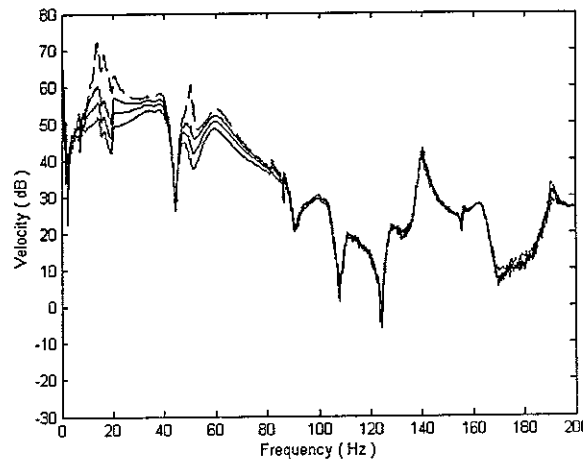

(b) Experiment

Figure 42 Velocity response at node 1 with single channel control implemented at node 1

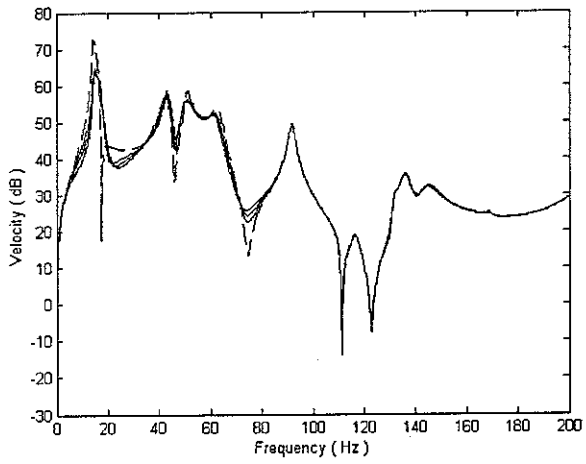

(a) Prediction

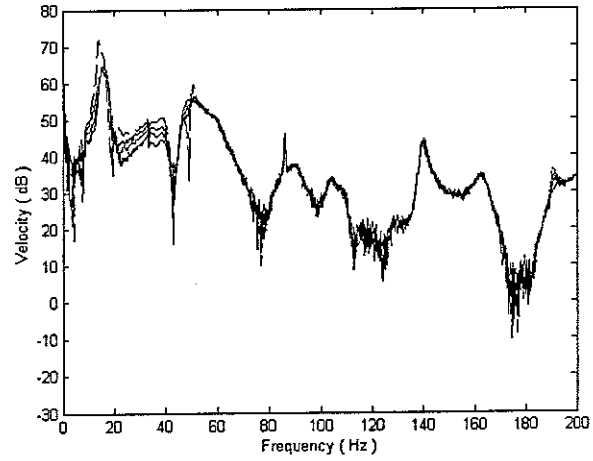

(b) Experiment

Figure 43 Velocity response at node 2 with single channel control implemented at node 1

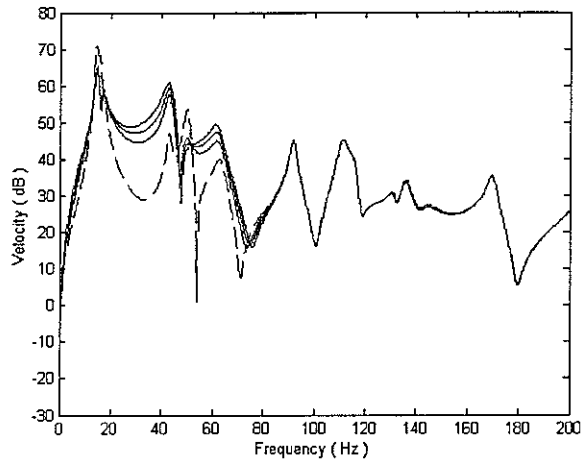

(a) Prediction

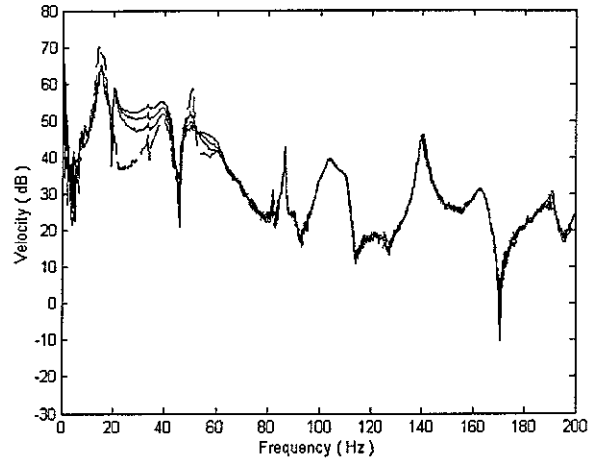

(b) Experiment

Figure 44 Velocity response at node 3 with single channel control implemented at node 1

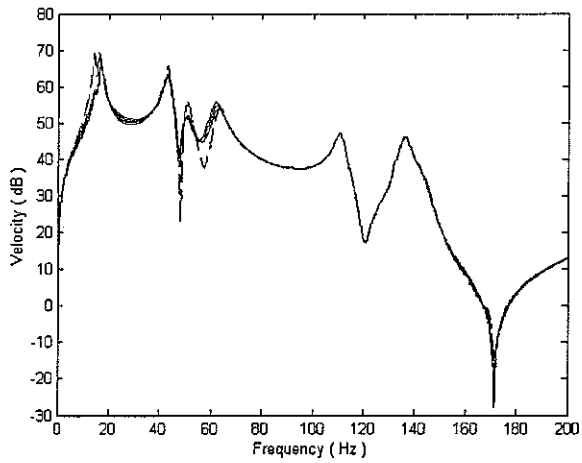

(a) Prediction

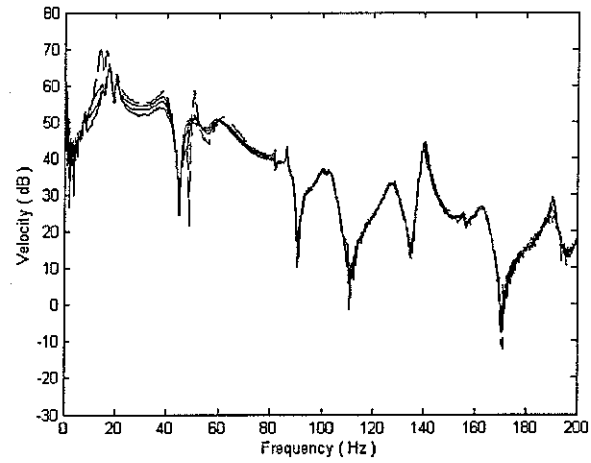

(b) Experiment

Figure 45 Velocity response at node 4 with single channel control implemented at node 1

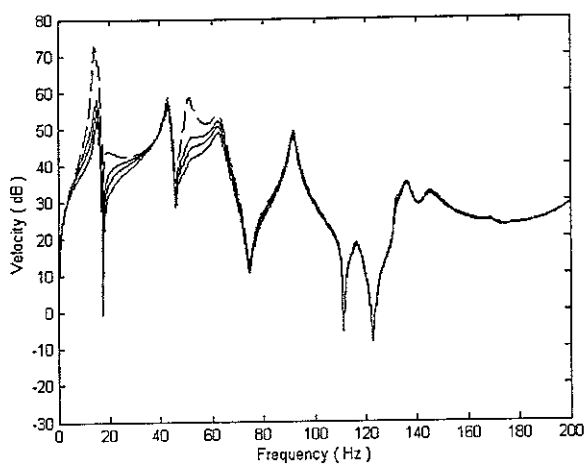

(a) Prediction

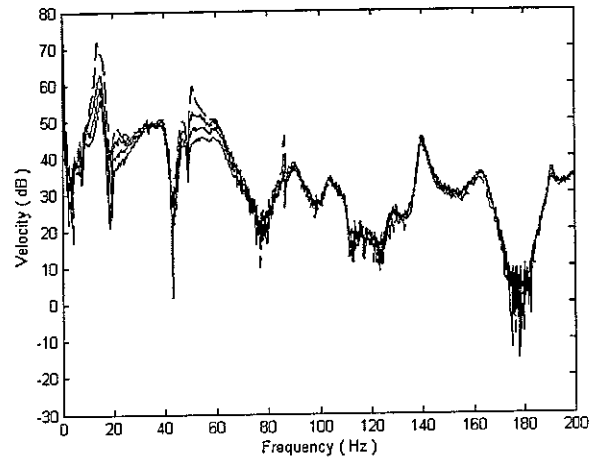

(b) Experiment

Figure 46 Velocity response at node 2 with single channel control implemented at node 2

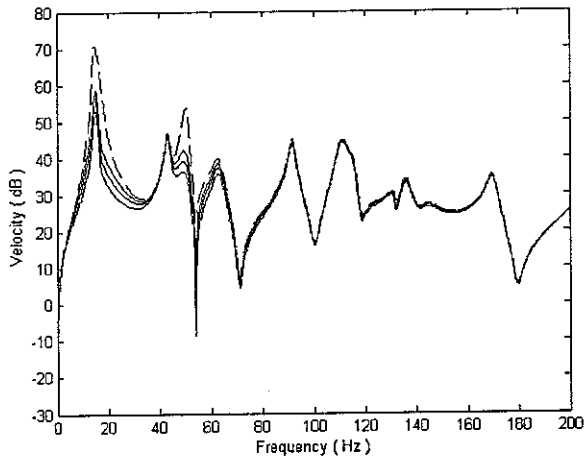

(a) Prediction

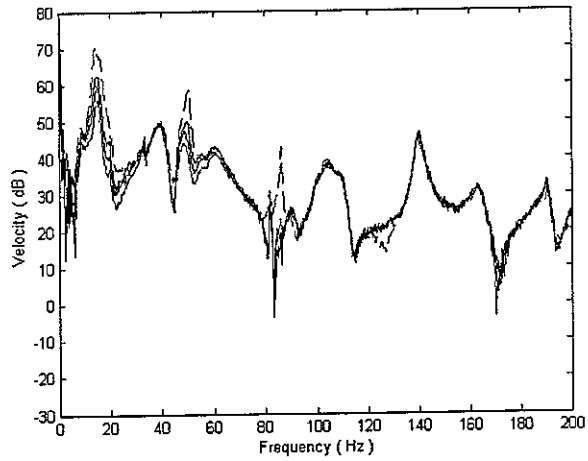

(b) Experiment

Figure 47 Velocity response at node 3 with single channel control implemented at node 3

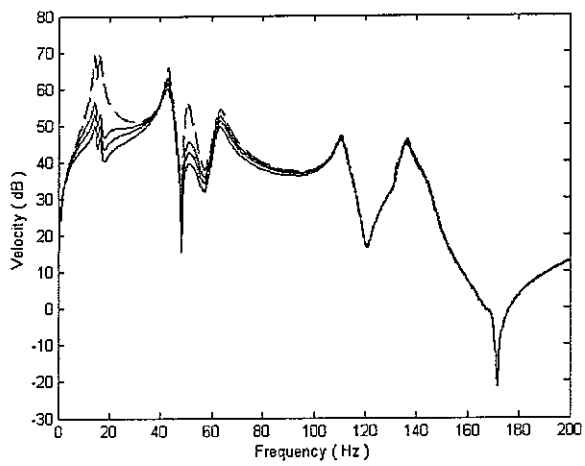

(a) Prediction

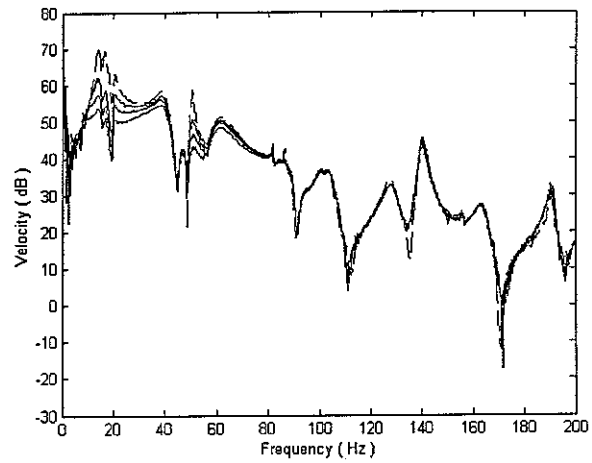

(b) Experiment

Figure 48 Velocity response at node 4 with single channel control implemented at node 4

7.2 Four-channel velocity feedback control implementation

The active vibration isolation of the mounted flexible equipment structure on the flexible base was investigated when four independent SISO controller were implemented at each mount position using an equal constant gain. The control performance was presented and assessed in terms of the absolute equipment velocity in this section.

The velocity responses at each node before control (in dashed lines) and after control (in solid lines) were shown both theoretically and experimentally from Figures 49 to 52 (dB ref.=10^{-5} m/s). The three solid curves in these figures corresponded to three different feedback control gain values of 0.182, 0.910 and 2.002 Ns/m respectively, which were calculated from the gain values of 2, 10, and 22 from the power amplifier and a gain of 100 mv per ms^{-1} from the charge amplifier. It is evident that the vibration amplitude is effectively reduced at all resonance frequencies of the mounted equipment structure within the frequency band of interest both theoretically and experimentally. The larger the feedback control gain, the greater reduction in the vibration level. Good stability of the four-channel control system is observed as the maximum feedback control gain of 11.83 Ns/m can be applied before the control system goes unstable. In other words, a gain margin of about 15 dB is obtained for the four-channel velocity feedback control system. The control performance predicted from the simulation agrees reasonably well with the experimental results except at very low frequency due to phase shifts.

In particular, up to 25 dB reduction in vibration levels at the rigid body modes of around 17 Hz, as well as up to 20 dB at the first flexible mode of 50.5 Hz, can be achieved in practice with a feedback control gain of 2.002 Ns/m. Amplifications of the very low frequency velocity responses of the flexible equipment structure can be observed in the experiments due to the effect of phase shifts. However, these effects are very small and no instability was encountered for these multiple feedback gains used in practice. However, instability does occur if the feedback gain is beyond the reported gain margin. For the vibrations at the base plate resonance frequency, different levels of attenuation were obtained at different mount positions. At nodes 1 and 4, the vibration levels at all base plate resonance frequencies were effectively reduced both theoretically and experimentally. However, exceptions occurred at nodes 2 and 3. At several base resonance frequencies the vibration was actually amplified in practice as clearly seen from Figure 51 at about 33 Hz at node 3. Similar observations were predicted from the simulation at the corresponding base resonance frequency of around 43 Hz at node 3 as shown in Figure 51. Thus, the individual absolute equipment velocity at each mount location is no longer suitable for assessing the control performance when the active vibration isolation system is installed on a flexible base structure. Alternatively, an approximate estimate of the kinetic energy represented by the sum of square values of the equipment velocities at all four mount locations is employed to assess the control performance of the active isolation system.

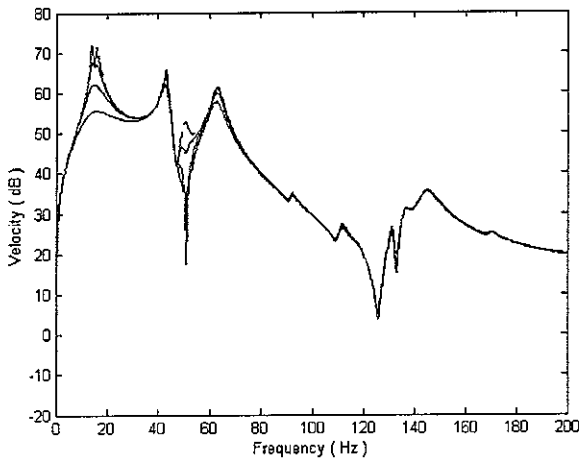

(a) Prediction

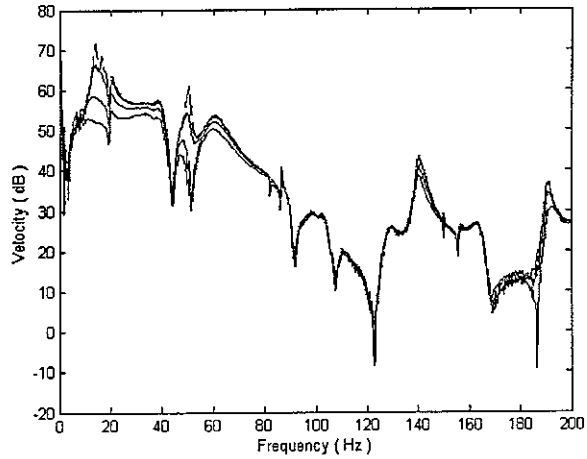

(b) Experiment

Figure 49 Velocity response at node 1 with four-channel control

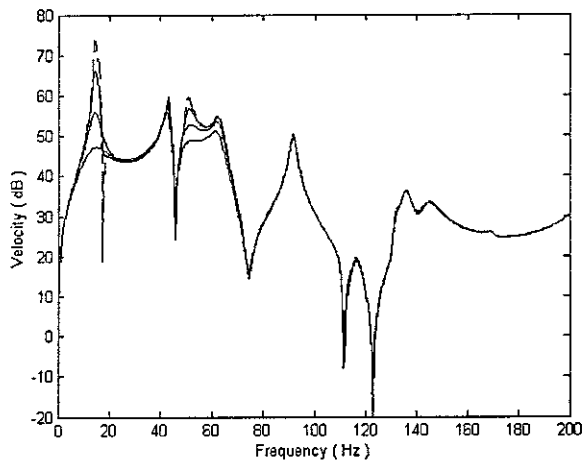

(a) Prediction

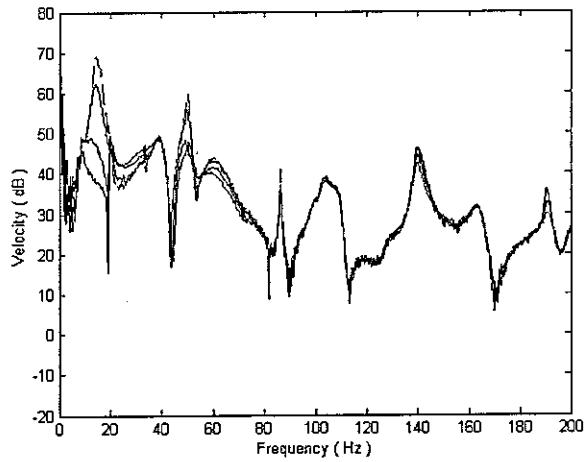

(b) Experiment

Figure 50 Velocity response at node 2 with four-channel control

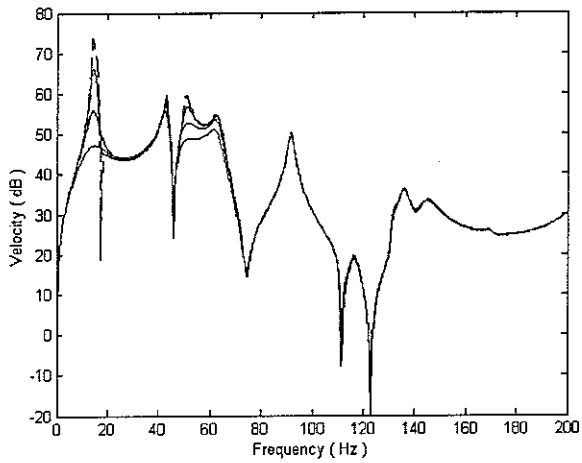

(a) Prediction

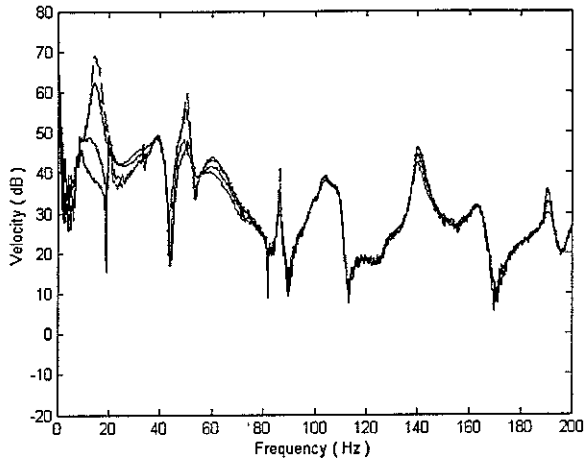

(b) Experiment

Figure 51 Velocity response at node 3 with four-channel control

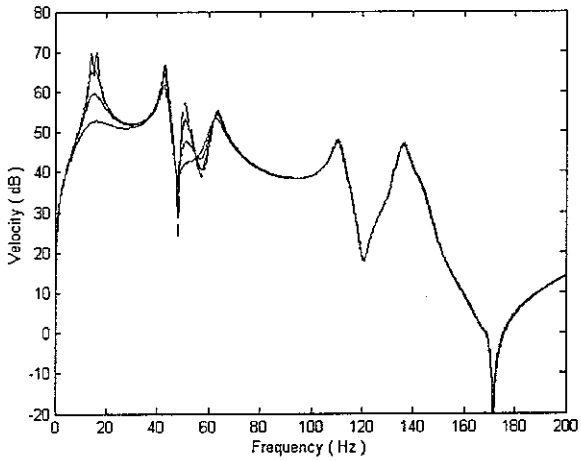

(a) Prediction

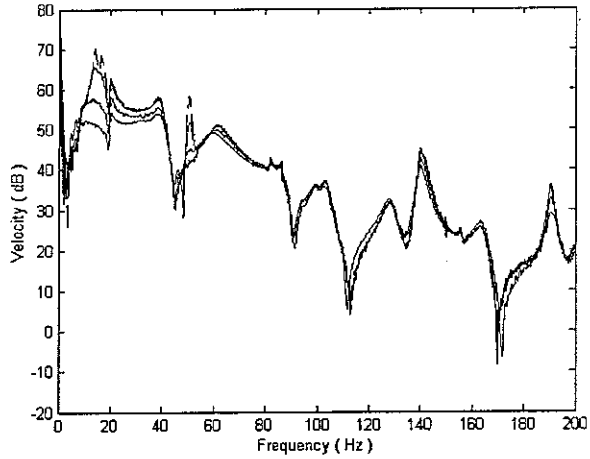

(b) Experiment

Figure 52 Velocity response at node 4 with four-channel control

7.3 Control performance assessed by the sum of squared velocities

Kim et al [6] adopted the kinetic energy as a measure of control performance for the active vibration isolation with a rigid equipment structure. Considering the flexibility of the equipment structure in this work, an approximate estimate of the kinetic energy represented by the sum of square values of the equipment velocities at each mount location is employed to assess the control performance of the active vibration isolation system. As a result, the sums of square values of equipment velocities obtained from the single channel and multichannel velocity feedback control systems were calculated and compared between the experiments and simulations to evaluate the control performances of the active isolation of the mounted flexible equipment structure from the vibration of a flexible base structure.

The sums of square values of the equipment velocities were shown in Figure 53 for the single channel control system and in Figure 54 for the multichannel control system (dB ref.=10^{-10} m/s). The results before control are illustrated in dashed lines, while the corresponding values after control are in solid lines. The three solid curves corresponded to three different feedback control gains respectively as described in the previous sections. It is demonstrated both theoretically and experimentally in Figure 53 that the implementation of a single channel control can effectively reduce the vibration levels at the resonance frequencies of the mounted equipment structure. However, amplifications are observed at the resonance frequencies of the base plate above 80 Hz from the simulation although it is difficult to see from Figure 53 (a). In practice, similar amplifications are observed when a single channel control system is implemented. The limitations are removed when a four-channel feedback control system is implemented for the mounted equipment structure as demonstrated in Figure 54. It is clearly shown both theoretically and experimentally that the vibration level has been effectively attenuated all over the frequency range of interest. In particular, up to 25 dB reductions in the kinetic energy at the rigid body modes of the mounted equipment structure, as well as up to 20 dB reduction at the resonances caused by the low order flexible modes of the coupled base and equipment structures, can be achieved in practice. In summery, the multichannel decentralised velocity feedback control system is very effective in attenuating the vibration levels of the mounted flexible equipment structure on a flexible base plate in the frequency band of analysis.

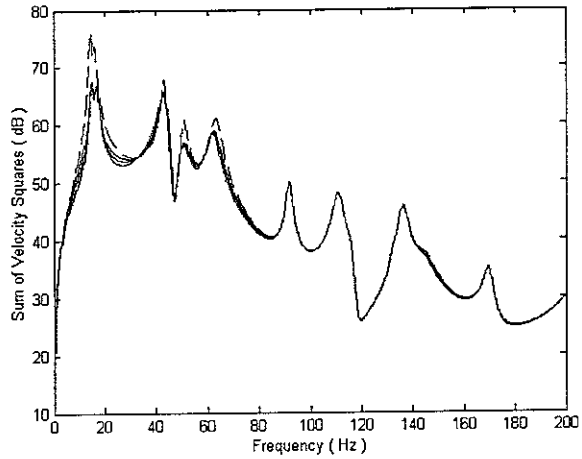

(a) Prediction

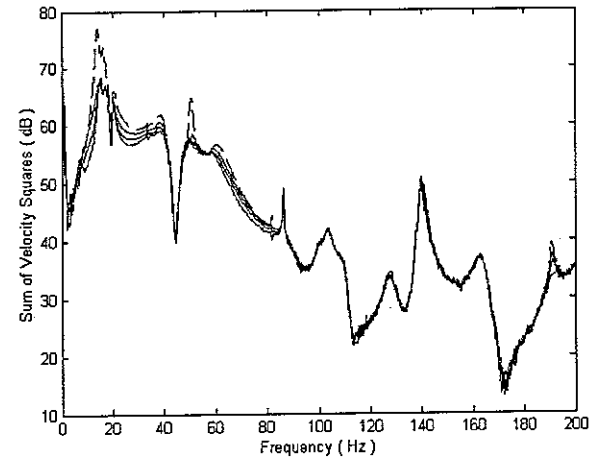

(b) Experiment

Figure 53 Sum of square values of equipment velocity for a single channel control at node 1

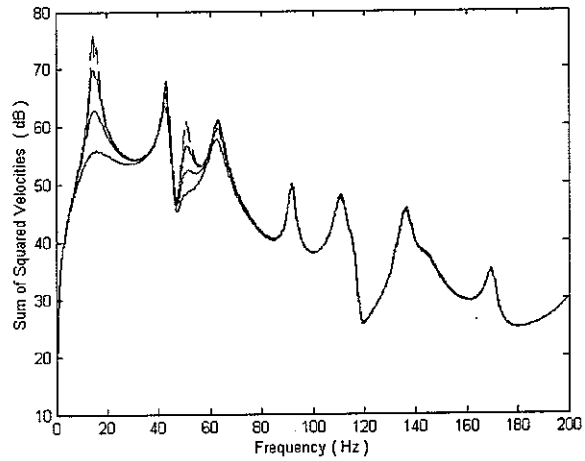

(a) Prediction

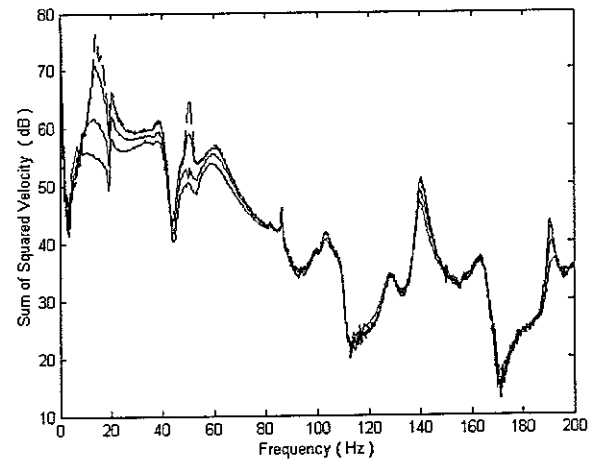

(b) Experiment

Figure 54 Sum of square values of equipment velocity for a four-channel control system

8 Conclusions

The objective of this work was to investigate the active isolation of a four-mount flexible equipment structure from a vibrating base structure. The dynamics and control mechanisms of the mounted flexible equipment structure on a flexible base plate have been studied theoretically and experimentally. The equipment velocity responses measured from the experiments agree reasonably well with the predicted results, which demonstrates that the theoretical model can be used to help to understand the dynamics and the active vibration control of the mounted flexible equipment structure on a flexible base. Good stability properties of the multichannel decentralised velocity feedback control system with a flexible equipment structure, as well as various single channel velocity feedback control systems, are predicted from the simulations and verified in the experimental implementations.

Control performances of the multichannel active vibration isolation system, as well as various single channel control systems, were assessed using an approximate estimate of the kinetic energy represented by the sum of the square values of equipment velocities at the mount positions. It is found from the simulations and experiments, that a single channel control can only effectively attenuate the vibration levels at the resonance frequencies of the mounted equipment structure, while amplifications of vibration at some of the base resonances are generally observed. The implementation of a multichannel velocity feedback control system presents much better control performance both theoretically and experimentally, with a global attenuation in the vibration levels of the flexible equipment structure at all resonance frequencies of analysis. In particular, up to 25 dB reductions in the kinetic energy at the rigid body modes of the mounted equipment structure, as well as up to 20 dB reduction at the resonances caused by the low order flexible modes of the coupled base and equipment structures, can be achieved in practice. In conclusion, the multichannel decentralised velocity feedback control system is effective in attenuating the vibration levels of a flexible equipment structure from a vibrating base structure in the frequency band of analysis.

References

1. C.E. Crede and J.E. Ruzicka,1996, Shock and Vibration Handbook (C.M. Harris, editor) New York: McGraw-Hill. Ch.30 Theory of vibration isolation.
2. M. Serrand and S.J. Elliott, 2000,Journal of Sound and Vibration, Vol. 234(4), 681-704, Multichannel feedback control for the isolation of base-excited vibration.
3. S M Kim, S J Elliott and M J Brennan 2001, IEEE Transactions on Control Systems Technology, 9(1). Decentralised control for multichannel active vibration isolation.
4. X. Huang, S.J. Elliott and M.J. Brennan, 2001, Institute of Sound and Vibration Research Technical Memorandum No 866, University of Southampton. Active Vibration Isolation of a flexible equipment structure on a rigid base.
5 G. B. Warburton, 1951, Proceedings of the Institute of Mechanical Engineering, Vol. 168, pp 371-384, The vibration of rectangular plates.
6. S. Skogestad and I. Postlethwaite, 1996, Multivariable feedback control: Analysis and Design, John Wiley & Sons, Inc.